ChemPubSoc Europe

DOI: 10.1002/cplu.201200244

Iron(II) α-Aminopyridine Complexes and Their Catalytic Activity in Oxidation Reactions: A Comparative Study of Activity and Ligand Decomposition

Matthew Lenze,[a] Erin T. Martin,[a] Nigam P. Rath,[a, b] and Eike B. Bauer*[a]

New well-defined Fe^{II} complexes bearing bi- and tridentate α-aminopyridine ligands were synthesized, and their catalytic activity in the oxidation of hydrocarbons and alcohols utilizing peroxide oxidants was investigated. The tridendate bis(picolyl)amine ligand **6** and its benzylated analogue **7** were converted into complexes $[Fe^{II}(\mathbf{6})_2]OTf_2$ (96%, X-ray; OTf = $CF_3SO_3^-$) and $[Fe^{II}(\mathbf{7})_2]OTf_2$ (90%). The bidentate aminopyridine ligand **8** was converted into $[Fe^{II}(\mathbf{8})_2(OTf)_2]$ (93%, X-ray). The new complexes are catalytically active in the oxidation of secondary alcohols and benzylic methylene groups to the corresponding ketones, of toluene to benzaldehyde, and of cyclohexene to cyclohexene oxide (3 mol% catalyst, *t*BuOOH (4 equiv), RT, 2–6 h, 28 to 85% yield of isolated product). The catalytic oxidation of cyclohexane with ROOH (R = H, *t*Bu) to an alcohol/ketone mixture with low ratio revealed that these oxidations follow largely a radical mechanism, except when $[Fe^{II}(\mathbf{6})_2]OTf_2$ was employed and H_2O_2 was added slowly. Together with known bi- and tetradendate iron complexes, a comparative study showed slight reactivity differences for the newly prepared complexes, with the highest observed for $[Fe^{II}(\mathbf{6})_2]OTf_2$ and $[Fe^{II}(\mathbf{7})_2]OTf_2$. The reaction of the new complexes with peroxides was followed over time by UV/Visible spectroscopy; this revealed a fast reaction between the two reactants within minutes. Ligand-decomposition pathways were investigated, and revealed that the NCH_2 units of the complexes are rapidly oxidized to the corresponding amides NC=O. The iron complex $[Fe^{II}(\mathbf{6})_2]OTf_2$ showed no decrease in catalytic activity and a moderate decrease in selectivity when first subjected to oxidative conditions similar to those employed in catalysis. Thus, oxidative ligand deterioration had a marginal effect on the catalytic activity of the iron complex $[Fe^{II}(\mathbf{6})_2]OTf_2$.

Introduction

Iron catalysis has emerged as a lively area of research in recent years.[1] Iron is less toxic than other transition metals typically utilized in catalysis and, owing to its abundance, it is readily available at a reasonable cost. Consequently, iron salts or complexes have been increasingly applied as catalysts in a variety of organic transformations, such as in C–C,[2] C–N,[3] and C–P[4] bond-forming reactions, heteroatom–heteroatom bond-forming reactions,[5] reductions,[6] and polymerizations[7] as well as other functional-group interconversions.[8]

Iron-based systems have also been investigated as catalysts in oxidation reactions of organic substrates. Fenton chemistry—that is, the oxidative power of iron salts in combination with peroxides—has been known for over 100 years.[9] Gif and GoAgg chemistry was popularized at the beginning of the 1980s by Barton and utilizes similarly simple conditions: the combination of iron or iron salts and acetic acid in pyridine that oxidatively functionalizes alkanes utilizing dioxygen or peroxides as the terminal oxidants.[10] The mechanism for both systems is still the objective of current research,[11] and the nonradical mechanism originally suggested by Barton[12] has been subsequently challenged.[13] Owing to the possible involvement of radicals in Fenton and Gif chemistry, their applicability in the synthesis of complex organic molecules is limited. Consequently, these systems have not been employed extensively in the synthesis of fine chemicals, and Fenton chemistry is utilized for wastewater treatment, in which the oxidative decomposition of organic compounds in solution is the final goal.[14]

Hence, recent research efforts have been directed towards iron catalysts that can be utilized in synthetically useful oxidation reactions under milder conditions in a more predictable manner. These research efforts are inspired by heme and nonheme enzymes such as the cytochrome P450 family[15] or the

[a] *M. Lenze, E. T. Martin, Dr. N. P. Rath, Prof. Dr. E. B. Bauer*
University of Missouri-St. Louis
Department of Chemistry and Biochemistry
One University Boulevard, St. Louis, MO 63121 (USA)
Fax: (+1) (314)-516-5342
E-mail: bauere@umsl.edu

[b] *Dr. N. P. Rath*
Center for Nanoscience, University of Missouri-St. Louis
St. Louis, MO 63121 (USA)

Supporting information for this article is available on the WWW under http://dx.doi.org/10.1002/cplu.201200244. It contains details of the typical experiment used to determine the alcohol/ketone ratios in Table 4; the experimental procedure to determine the activities in Figure 3; the experimental procedure to record the time-resolved UV/Visible spectra of the metal complexes after addition of the oxidant in Figures 4, 5, and 6; the representative experimental procedure to determine ligand-decomposition pathways; experimental details, characterization data, and ^1H and $^{13}C\{^1H\}$ NMR spectra for the catalysis products; ^1H NMR and UV/Visible spectra of all metal complexes; GC–MS traces of the ligand-decomposition reactions in Scheme 4.

methane monooxygenase[16] that can be found in nature. These enzymes accomplish oxidation reactions under physiological conditions, and feature well-defined, iron-containing cofactors bearing N-coordinating ligands in their coordination sphere. Research efforts have been targeted towards artificial iron complexes mimicking the active sites of the enzymes found in nature.[15–17] These research efforts afforded a number of catalyst systems that show high efficiencies and selectivities in oxidation reactions.[18] Some of these complexes are formed in situ[19] and have been successfully employed in the oxidation of alkanes,[20] benzylic methylene groups,[21] and alcohols;[22] in oxidative cleavage reactions;[23] and in the epoxidation of alkenes.[24] It appears that well-defined, preformed nonheme iron complexes perform notably well in oxidation reactions, for example, White's iron complex **5**, which selectively oxidizes tertiary CH units to the corresponding alcohols.[25] Iron complexes of the tris(2-picolyl)amine (tpa) ligands **1** and BPMEN (**2a**) were utilized by Que for alkane oxidations with high alcohol/ketone ratios.[26] The ligands **2b–d**,[27] **3**,[28] and bispidine[29] have also been employed in the synthesis of well-defined, catalytically active iron complexes, and, as a consequence, the application of these systems in the synthesis of complex organic molecules has become increasingly popular.[30]

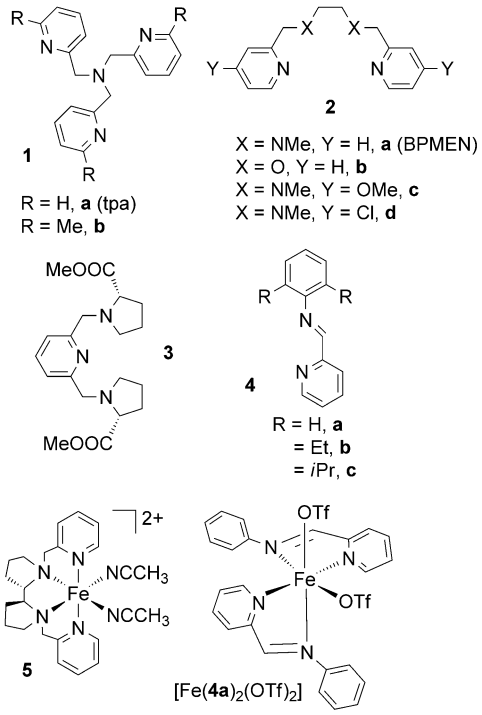

Still, existing oxidation systems suffer from some drawbacks, such as insufficient turnover numbers (TONs) or selectivities.[20b,31] Potential issues are the involvement of radicals in the course of the oxidation reactions and oxidative ligand-decomposition pathways, which potentially can lead to catalyst deactivation.[32] The search for improved iron-based catalyst systems for oxidation reactions utilizing peroxide oxidants is, thus, ongoing.

As part of our long-standing research interest in iron-based catalysis, we are especially interested in how the ligand structure can impair the catalytic activity of an iron complex.[33] We recently reported a series of iron complexes $[Fe(\mathbf{4})_2(OTf)_2]$ ($OTf = CF_3SO_3^-$) bearing α-imino pyridine ligands **4**, which we successfully employed as catalysts in the oxidation of activated methylene groups and secondary alcohols with *t*BuOOH to obtain the corresponding ketones (4 h, RT, 3% catalyst loading, 22–91% yield of isolated product).[33a] Sterically and electronically tuned ligands **4** were employed in the synthesis of the corresponding α-imino pyridine iron complexes; however, such tuning efforts had only limited impact on the catalytic activity, which was comparable for all complexes of that specific library. We speculated that ligand architectures could impair the catalytic activity of complexes, and decided to compare the efficiency of different types of ligands in iron-based oxidation systems.

Herein, we describe the synthesis and characterization of new iron mono- and bis(2-picolyl)amine complexes and their catalytic activity. We compare the activities of these new complexes with those of known complexes previously employed in the title reactions. We furthermore report ligand-decomposition pathways for the iron complexes and how such ligand deterioration impairs the activity of the catalyst system. Finally, mechanistic studies were performed to identify intermediates and to assess to what extent radicals may be involved in the reactions.

Results

Synthesis of new iron complexes

For comparative studies, we first selected a set of nitrogen-based ligands that differ significantly in their architecture and denticity and converted them to their respective iron complexes. The tpa complex $[Fe^{II}(\mathbf{1a})(OTf)_2]$ is known and was synthesized according to literature procedures,[34] and will subsequently be referred to as $[Fe^{II}(tpa)(OTf)_2]$. Likewise, complex $[Fe^{II}(\mathbf{4a})_2(OTf)_2]$ has been synthesized and characterized previously in our laboratory.[33a]

To investigate different denticities, we utilized the commercial, tridentate bis(2-pyridinylmethyl)amine (bpa) ligand **6** (Scheme 1). This ligand has been converted previously to iron complexes of the formula $[Fe^{III}(\mathbf{6})Cl_3]$[35] and $[Fe^{II}(\mathbf{6})_2]X_2$ ($X = Cl^-$, Br^-),[36] and their utilization as catalysts in oxidation reactions is about to emerge.[37] It is known that $\mathbf{L}_nFe^{III}$ complexes can form relatively stable oxo-bridged iron dimers of the general formula $[\mathbf{L}_nFe{-}O{-}Fe\mathbf{L}_n]$.[38] Complex $[Fe^{II}(\mathbf{6})_2]Cl_2$ dimerizes in solution and is oxidized in the air to an oxo-bridged Fe^{III} dimer.[36b] Some oxo-bridged iron complexes show catalytic activity in alkane oxidations;[39] however, they tend to be less efficient than the enzymes found in nature,[40] and the stability reported for some of these systems might, in the present context, slow down or inhibit catalytic cycles. Simple halide counterions can firmly coordinate to the iron center and impede substrate coordination to the metal; for this reason, complex $[Fe^{III}(tpa)Cl_2](ClO_4)$ did not catalyze the oxidation of cyclohexane utilizing H_2O_2.[26] Preliminary data from our own laboratory also showed that complex $[Fe^{II}(\mathbf{6})_2]Cl_2$ exhibited low catalytic activity in oxi-

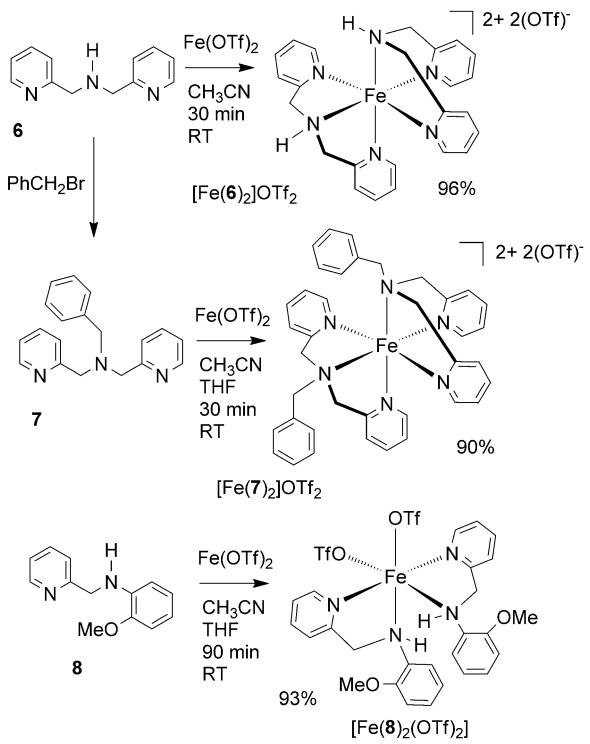

Scheme 1. Synthesis of iron complexes.

dation reactions and its chemistry was, thus, not pursued further.

Therefore, next we targeted iron complex $[Fe^{II}(\mathbf{6})_2]OTf_2$, which features OTf ($=CF_3SO_3^-$), a readily displaceable counterion, and two tridentate bpa ligands **6** in its coordination sphere, potentially inhibiting bimolecular decomposition pathways[41] and the formation of stable oxo-bridged dimers. $[Fe^{II}(\mathbf{6})_2]OTf_2$ was obtained by combining $[Fe^{II}(OTf)_2]$ and two equivalents of **6** in CH_3CN. Crystallization with diethyl ether afforded iron complex $[Fe^{II}(\mathbf{6})_2]OTf_2$ as a red solid in 96% yield (Scheme 1).

The acidity of the N–H unit in **6** might increase significantly upon coordination to a metal center. To investigate the influence of the N–H unit on the catalytic activity, we replaced the hydrogen in ligand **6** by a benzyl group, affording the known[42] bis(2-pyridylmethyl)benzyl amine (bpba) ligand **7**. It has been employed previously in the synthesis of oxo-bridged diiron complexes of the general formula $[Fe^{III}_2(O)(OOR)(\mathbf{7})](ClO_4)_2$.[40] However, to the best of our knowledge, the related complex $[Fe^{II}(\mathbf{7})_2]OTf_2$ has not yet been reported. Combining two equivalents of ligand **7** and one equivalent of $[Fe^{II}(OTf)_2]$ afforded, after workup by crystallization, complex $[Fe^{II}(\mathbf{7})_2]OTf_2$ in 90% yield as a red-tan powder.

It has been suggested in the literature that two tridentate ligands in the coordination sphere of iron complexes might inhibit catalytic cycles, as they occupy all six coordination sites at the metal center.[43] For direct comparison with imine ligands **4**, we synthesized bidentate α-aminopyridyl ligand **8** by reductive amination of 2-pyridine carboxaldehyde with 2-methoxyaniline by following a literature procedure for the related ligand **6**.[35a] Ligand **8** was converted in a procedure similar to those described above to the iron complex $[Fe^{II}(\mathbf{8})_2(OTf)_2]$, which was obtained as a purple solid in 93% yield of isolated product. We also tried to convert other α-aminopyridyl ligands to their respective iron complexes, but solubility issues rendered workup efforts and catalytic applications impossible.

Characterization of the new iron complexes

The new complexes $[Fe^{II}(\mathbf{6})_2]OTf_2$, $[Fe^{II}(\mathbf{7})_2]OTf_2$, and $[Fe^{II}(\mathbf{8})_2(OTf)_2]$ were analyzed by MS, IR, X-ray diffraction, UV/Visible, ^1H and ^{19}F NMR spectroscopy, magnetic measurements, and elemental analyses. The NMR spectroscopy, UV/Visible, magnetic moment, and IR data for the complexes are compiled in Table 1.

Complex $[Fe^{II}(\mathbf{6})_2]OTf_2$ has been synthesized previously with bromide[36a] and iodide counterions.[36b] However, none of these previously reported complexes have been analyzed by NMR spectroscopy and were reported to adopt a low-spin configuration.[36] Complex $[Fe^{II}(\mathbf{6})_2]OTf_2$ exhibited a magnetic moment ($\mu_{eff}=1.83$ BM, determined with a magnetic susceptibility balance) and features well-resolved ^1H and ^{13}C NMR spectra in the diamagnetic regions. However, some line broadening was observed in the ^1H NMR spectrum, and it was not in complete agreement with the structure shown in Scheme 1 (as determined by X-ray diffraction, see below). In addition, the magnetic moment is not exactly zero as expected for a low-spin Fe^{II} complex. Thus, we recorded low-temperature ^1H NMR spectra (provided in the Supporting Information), and at −50 °C, a new set of sharp signals appeared in the spectrum, which is in agreement with the structure of $[Fe^{II}(\mathbf{6})_2]OTf_2$ as shown in Scheme 1. It appears that the complex exhibits dynamic behavior at room temperature. The *trans* isomers were determined by X-ray diffraction for $[Fe^{II}(\mathbf{6})_2]Br_2$ and $[Fe^{II}(\mathbf{6})_2]Cl_2$.[36] The dynamic behavior of $[Fe^{II}(\mathbf{6})_2]OTf_2$ at room temperature might explain its intermediate effective magnetic moment of 1.83 BM.

Table 1. Selected physical data of the new iron complexes.

	IR, ν_{NH} [cm^{-1}]	UV/Visible[a]		Magnetic moments[b]	^{19}F NMR	
	free ligand/complex	λ_{max} [CH_2Cl_2] [nm]	ε [$M^{-1}cm^{-1}$]	μ_{eff} [BM]	δ [ppm]	$\nu_{1/2}$ [Hz]
$[Fe^{II}(\mathbf{6})_2]^{2+}$	3316/3245	435	7450 (MLCT)	1.83	−78	38
$[Fe^{II}(\mathbf{7})_2]^{2+}$	–/–	≈550	≪100 (d–d)	4.40	−79	36
$[Fe^{II}(\mathbf{8})_2]^{2+}$	3391/3248	≈550	≪100 (d–d)	4.63	−64	5100

[a] In CH_3CN, with concentrations ranging from 0.3×10^{-3} to 1.4×10^{-3} M. [b] In the solid state at 298 K, determined with a magnetic susceptibility balance.

Complex $[Fe^{II}(\mathbf{7})_2]OTf_2$ also bears two tridentate ligands **7** in its coordination sphere, and two OTf anions serve as counterions, as confirmed by elemental analysis, ^{19}F NMR spectroscopy, and MS. As opposed to $[Fe^{II}(\mathbf{6})_2]OTf_2$, complex $[Fe^{II}(\mathbf{7})_2]OTf_2$ is paramagnetic ($\mu_{eff} = 4.40$ BM). As a consequence, its ^1H NMR spectrum shows large paramagnetic shifts between $\delta = -20$ and 120 ppm, which have previously been reported in the literature for related high-spin Fe^{II} systems, and often not all resonances can be observed.[27a,33a]

The aminopyridyl complex $[Fe^{II}(\mathbf{8})_2(OTf)_2]$ bears two bidentate ligands **8** and two OTf ligands in the coordination sphere. This complex is also paramagnetic ($\mu_{eff} = 4.63$ BM), and features large paramagnetic shifts between $\delta = 0$ and 120 ppm in the ^1H NMR spectrum. The general formulation $[Fe^{II}(\mathbf{8})_2(OTf)_2]$ is also confirmed by elemental analysis and MS.

To assess the position of the OTf counterion in solution, ^{19}F NMR spectra of the three complexes were recorded in CD_3CN. Non-coordinated OTf counterions give solvent-dependent resonances around $\delta = -70$ ppm that shift significantly downfield upon coordination to Fe^{II}.[44] In complexes $[Fe^{II}(\mathbf{6})_2]OTf_2$ and $[Fe^{II}(\mathbf{7})_2]OTf_2$, the ^{19}F NMR spectra resonances were observed between $\delta = -78$ and -79 ppm (Table 1), which is consistent with free, non-coordinated OTf. The widths at half height ($\nu_{1/2}$) for the ^{19}F NMR spectroscopic resonances for the two complexes are 38 and 36 Hz for the two complexes, respectively. The small widths at half-height are indicative of the absence of dynamic processes in solution involving the OTf counterion,[27a] as all six coordination sites are occupied by the two tridentate ligands.

In the amino pyridine complex $[Fe^{II}(\mathbf{8})_2(OTf)_2]$, two coordination sites are occupied by the weakly coordinating OTf anion, and its ^{19}F NMR spectrum exhibited a very broad resonance around $\delta = -64$ ppm ($\nu_{1/2} \approx 5100$ Hz). The OTf ligand appears to rapidly exchange with the CD_3CN solvent, which leads to significant line broadening of the resonance. The large $\nu_{1/2}$ value is indicative of dynamic processes in solution involving the OTf counterion.[27a]

The UV/Visible spectra of the three complexes were recorded in CH_3CN and CH_2Cl_2, and only $[Fe^{II}(\mathbf{6})_2]OTf_2$ features a metal-to-ligand charge transfer (MLCT) band at $\lambda = 435$ nm (Table 1 and Figure 1, which shows the traces recorded in CH_3CN). The molar absorptivity ε of the MLCT band is 7450 $M^{-1}cm^{-1}$ in CH_3CN and is typical for MLCT bands (solid trace in Figure 1); both the wavelengths and the high values for the molar absorptivity are typical for Fe^{II} complexes with N-coordinating donor ligands and have been reported previously for structurally related species.[27a,33a,45] The UV/Visible spectra barely changed when recorded in non-coordinating CH_2Cl_2 (the spectra are given in the Supporting Information). The similarities of the UV/Visible spectra in coordinating CH_3CN and non-coordinating CH_2Cl_2 suggest that the structure of the complexes in solution are identical, that is, the CH_3CN solvent itself does not displace the ligands or one of its coordinating N-donor atoms; similar conclusions were drawn from UV/Visible data for related iron complexes with nitrogen-donor atoms.[41] The other two complexes $[Fe^{II}(\mathbf{7})_2]OTf_2$ and $[Fe^{II}(\mathbf{8})_2(OTf)_2]$ did not exhibit MLCT bands; they show very weak and broad absorbances around 550 nm, which could, owing to their low intensity ($\varepsilon \ll 100\ M^{-1}cm^{-1}$), be d–d transitions (dotted and dashed traces in Figure 1).[46]

The IR spectra of the new complexes exhibited strong bands for the OTf counteranion. Non-coordinated OTf typically exhibits IR stretches at 1268, 1223, 1143, and 1030 cm^{-1}; the solid-state IR spectra of the three complexes also showed four comparable signals; some of the signals are desymmetrized for $[Fe^{II}(\mathbf{8})_2(OTf)_2]$ and exhibited shoulders, as previously reported for OTf coordinated to metal centers.[33c,47] The complexes $[Fe^{II}(\mathbf{6})_2]OTf_2$ and $[Fe^{II}(\mathbf{8})_2(OTf)_2]$ feature N–H units in their ligands. Absorptions were observed at 3245 and 3248 cm^{-1}, respectively, which are about 100 cm^{-1} lower than the corresponding absorbances of the free ligands (Table 1). This shift in the absorbances indicates that the N–H unit is coordinated to the iron center.

To unequivocally establish the structures of the new iron complexes, the X-ray structures of complexes $[Fe^{II}(\mathbf{6})_2]OTf_2$ and $[Fe^{II}(\mathbf{8})_2(OTf)_2]$ were determined (Figure 2). Crystallographic parameters are given in Table 2 and key bond lengths and angles are compiled in Table 3.

For complex $[Fe^{II}(\mathbf{6})_2]OTf_2$, the bond angles for the N atoms in *cis* positions about the iron center range from 82.54(9) to

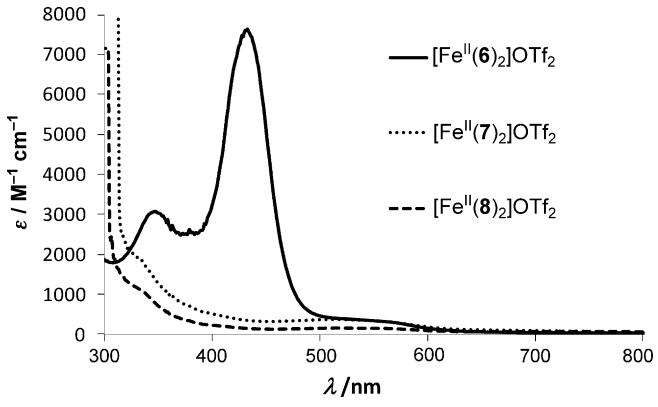

Figure 1. UV/Visible spectra of $[Fe^{II}(\mathbf{6})_2]OTf_2$ (solid line), $[Fe^{II}(\mathbf{7})_2]OTf_2$, and $[Fe^{II}(\mathbf{8})_2(OTf)_2]$.

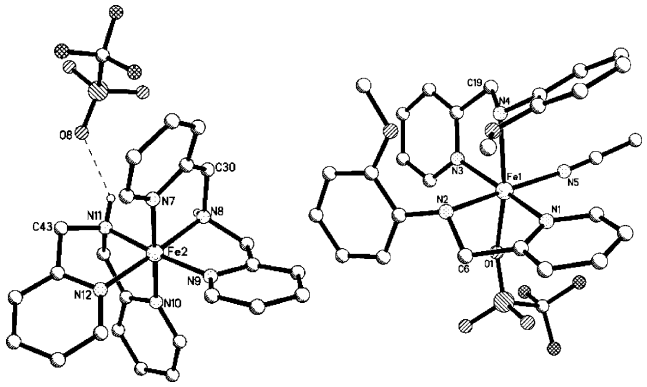

Figure 2. X-ray structures of $[Fe^{II}(\mathbf{6})_2]^{2+}\cdots OTf$ (left) and $[Fe^{II}(\mathbf{8})_2(OTf)(CH_3CN)]^+$ (right). Hydrogen atoms, solvent molecules, and one of the OTf counter ions have been omitted for clarity. Plots giving thermal ellipsoids are given in the Supporting Information.

Table 2. Crystallographic parameters.

	$[Fe^{II}(\mathbf{6})_2]OTf_2$	$[Fe^{II}(\mathbf{8})_2OTf_2]$
empirical formula	$C_{56}H_{58}F_{12}Fe_2N_{14}O_{12}S_4$	$C_{29}H_{31}F_3FeN_5O_5S\cdot(CH_3CN)(CF_3SO_3)$
M_r	1587.10	864.62
T [K]	100(2)	100(2)
λ [Å]	0.71073	0.71073
crystal system	monoclinic	triclinic
space group	P_n	$P\bar{1}$
a [Å]	16.9936(10)	10.5308(6)
b [Å]	9.3511(6)	13.4426(8)
c [Å]	20.5805(12)	13.9190(9)
α [°]	90	75.702(3)
β [°]	102.006(3)	77.494(3)
γ [°]	90	79.812(3)
V [Å^3]	3198.9(3)	1848.13(19)
Z	2	2
ρ_{calcd} [Mg m^{-3}]	1.648	1.554
μ [mm^{-1}]	0.692	0.609
$F(000)$	1624	888
crystal size [mm^3]	0.28×0.27×0.20	0.22×0.10×0.09
θ range for data collection [°]	2.02 to 32.18	1.95 to 26.60
index ranges	$-25\le h\le 25$ $-13\le k\le 13$ $-30\le l\le 30$	$-13\le h\le 12$ $-16\le k\le 16$ $-17\le l\le 17$
reflections collected	139854	42411
independent reflections	21639 [R(int) = 0.0636]	7510 [R(int) = 0.0521]
completeness to θ = 25.00° [%]	100.0	98.6
absorption correction	semi-empirical from equivalents	semi-empirical from equivalents
max. and min. transmission	0.8717 and 0.8277	0.9461 and 0.8791
refinement method	full-matrix least-squares on F^2	full-matrix least-squares on F^2
data/restraints/parameters	21639/15/937	7510/51/516
GOF on F^2	1.021	1.015
final R indices [$I>2\sigma(I)$]	R_1 = 0.0468, wR_2 = 0.1148	R_1 = 0.0391, wR_2 = 0.0822
R indices (all data)	R_1 = 0.0579, wR_2 = 0.1222	R_1 = 0.0629, wR_2 = 0.0921
absolute structure parameter	0.669(9)	
largest diff. peak and hole [e Å^{-3}]	1.381 and −0.761	0.696 and −0.483

Table 3. Key bond lengths [Å] and angles [°].

	$[Fe^{II}(\mathbf{6})_2]OTf_2$		$[Fe^{II}(\mathbf{8})_2]OTf_2$
Fe2–N7	1.964(2)	Fe1–N1	2.1463(19)
Fe2–N8	2.006(2)	Fe1–N2	2.257(2)
Fe2–N9	1.997(2)	Fe1–N3	2.1577(19)
Fe2–N10	1.986(2)	Fe1–N4	2.249(2)
Fe2–N11	2.011(2)	Fe1–N5	2.160(2)
Fe2–N12	1.990(2)	Fe1–O1	2.0879(17)
N11–C43	1.487(4)	N2–C6	1.474(3)
N8–C30	1.480(4)	N4–C19	1.458(3)
C29–C30	1.521(5)	C5–C6	1.497(3)
C43–C44	1.479(4)	C18–C19	1.499(3)
N8-Fe2-N9	82.51(10)	N1-Fe1-N2	76.37(7)
N9-Fe2-N10	97.02(9)	N2-Fe1-N3	94.71(7)
N7-Fe2-N11	94.33(10)	N1-Fe1-N5	94.08(8)
N7-Fe2-N10	178.06(8)	N1-Fe1-N3	169.42(7)
N8-Fe2-N12	175.45(10)	N2-Fe1-N5	169.47(7)
		N2-Fe1-O1	92.56(7)

98.26(9)° and those in *trans* positions range from 174.15(7) to 178.06(8)°. The structure is, thus, best described as distorted octahedral. The N-Fe-N bond angles within the ligands range from 82.54(9) to 85.78(9)°, whereas they range from 91.04(9) to 101.9(2)° between ligands. Thus, the average "bite angle" for ligand **6** is around 84°, which might be responsible for the distortion of the complex. The Fe–N bond lengths are between 1.984(2) and 2.011(2) Å, which are typical for low-spin Fe^{II} complexes. The two OTf counterions are not coordinated to the iron center. There is a hydrogen bond between the S–O units of the OTf and the N–H group of the ligand (Figure 2, left), ranging from 2.0 to 2.3 Å, which has been reported previously for related complexes with Cl^- or Br^- counterions.[36a] The bond lengths and angles for $[Fe^{II}(\mathbf{6})_2]OTf_2$ closely match the corresponding values of complexes $[Fe^{II}(\mathbf{6})_2]X_2$ (X = Cl^-, Br^-), which have been structurally characterized previously.[36] As outlined above, there is an interesting difference in the coordination mode of ligand **6** in these two complexes with halide counterions and in complex $[Fe^{II}(\mathbf{6})_2]OTf_2$. In complexes $[Fe^{II}(\mathbf{6})_2]X_2$ (X = Cl^-, Br^-), the two N–H groups occupy positions *trans* to each other.[36] However, the N–H units are located *cis* to each other in complex $[Fe^{II}(\mathbf{6})_2]OTf_2$, and *trans* to a pyridyl ring in the solid state. At room temperature, the complex shows dynamic behavior in solution, and it appears that the isomer with the N–H groups *cis* to each other crystallizes out of solution (the crystals for X-ray diffraction were grown at −18 °C). Complexes $[Fe^{II}(\mathbf{6})_2]Cl_2$ and $[Fe^{II}(\mathbf{6})_2]Br_2$ were not investigated by NMR spectroscopy in solution.[36] It is possible that those complexes also show dynamic behavior in solution at room temperature, but owing to the different counterions, the other isomers precipitate out of solution.

For complex $[Fe^{II}(\mathbf{8})_2(OTf)_2]$, the bond angles for N atoms in *cis* positions about the iron center range from 76.37(7) to 94.71(7)° and for those in the *trans* positions around 169.4°. The structure is, thus, also best described as distorted octahedral. The two N–H units are in *cis* positions to each other, as observed for complex $[Fe^{II}(\mathbf{6})_2]OTf_2$. The N-Fe-N bond angles within the ligands are 76.37(7) and 75.59(7)°, respectively, and 94.71(7) and 98.32(7)° between ligands. Thus, the average "bite angle" for the amino pyridyl ligand **8** is around 75°, also leading to the distortion of the octahedral coordination geometry for the complex. The Fe–N bond lengths are between 2.1463(19) and 2.257(2) Å, which are about 0.2 Å longer than those for $[Fe^{II}(\mathbf{6})_2]OTf_2$. Complex $[Fe^{II}(\mathbf{8})_2(OTf)_2]$ has a high-spin configuration as determined by magnetic measurements (Table 1), and it has previously been reported that Fe^{II}–N bond lengths for high-spin complexes are around 2.2 Å and about 0.2 Å longer than those of corresponding low-spin complexes.[26,33a] The X-ray structure of $[Fe^{II}(\mathbf{8})_2(OTf)_2]$ reveals that one of the OTf ions is coordinated to the metal center whereas the other one serves as the counterion. The remaining coordination site is occupied by a CH_3CN solvent molecule. In the originally isolated complex, there was no evidence for the presence of CH_3CN, as assessed by elemental analysis and IR data. We assume that its presence in the coordination sphere observed in the X-ray structure is a result of the crystallization procedure

employed to obtain X-ray-quality crystals, which involved CH_3CN as solvent.

The synthetic efforts described in this section afforded three well-defined iron complexes $[Fe^{II}(\mathbf{6})_2]OTf_2$, $[Fe^{II}(\mathbf{7})_2]OTf_2$, and $[Fe^{II}(\mathbf{8})_2(OTf)_2]$ which, with the previously synthesized complexes $[Fe^{II}(\mathbf{4a})_2(OTf)_2]$ and $[Fe^{II}(tpa)(OTf)_2]$ were subsequently employed in catalytic studies.

Catalysis and catalytic efficiency

The oxidation of cyclohexane is used frequently as a benchmark reaction to investigate catalytic selectivity and mechanistic pathways.[11a] In these test reactions, a large excess amount of the substrate over the peroxide oxidant is employed typically to avoid overoxidations.[28] The alcohol/ketone ratio of the oxidation products gives information about the course of the reaction, which is high for metal-centered mechanistic pathways and low for free-radical oxidation reactions (see below).[28] Accordingly, we employed various cyclohexane/H_2O_2 or cyclohexane/*t*BuOOH ratios and the relevant results are compiled in Table 4.

Table 4. Cyclohexane oxidation.[a]

	Reaction time [min]	Peroxide/substrate ratio	Alcohol/ketone ratio
	Cyclohexane oxidation with fast addition of H_2O_2[b]		
$[Fe^{II}(\mathbf{6})_2]^{2+}$	120	0.1	0.25
	240	0.1	0.25
$[Fe^{II}(\mathbf{7})_2]^{2+}$	120	0.1	0.25
$[Fe^{II}(\mathbf{8})_2(OTf)_2]$	120	0.1	0.33
	Cyclohexane oxidation with slow addition of H_2O_2[c]		
$[Fe^{II}(\mathbf{6})_2]^{2+}$	25	0.01	6.6
$[Fe^{II}(\mathbf{7})_2]^{2+}$	25	0.01	1.1
$[Fe^{II}(\mathbf{8})_2(OTf)_2]$	25	0.01	1.5
"**19**"	25	0.01	3.0
	Cyclohexane oxidation with *t*BuOOH (slow addition of a dilute solution)[c]		
$[Fe^{II}(\mathbf{6})_2]^{2+}$	25	0.1	0.5
$[Fe^{II}(\mathbf{7})_2]^{2+}$	25	0.1	0.66
$[Fe^{II}(\mathbf{8})_2(OTf)_2]$	25	0.1	0.66

[a] Peroxide/catalyst ratio = 10. Details are given in the Experimental Section. [b] Fast addition of H_2O_2 to the reaction mixture. [c] Slow addition over 25 min of a dilute 90 mM H_2O_2 or *t*BuOOH solution to the reaction mixture.

For the oxidation reactions with H_2O_2, the alcohol/ketone ratios obtained strongly depend on the cyclohexane/H_2O_2 ratio and the manner in which the peroxide oxidant was added to the reaction mixture. When the peroxide solution was added rapidly to a solution containing the cyclohexane substrate and the catalyst, a low alcohol/ketone ratio ranging from 0.25 to 0.33 was detected by GC, irrespective of the cyclohexane/oxidant ratio.

However, when H_2O_2 was added as a dilute solution of 90 mM over the course of 25 min by syringe pump to the reaction mixture at a 0.01 H_2O_2/cyclohexane ratio, the alcohol/ketone ratio was much higher (6.6) for $[Fe^{II}(\mathbf{6})_2]OTf_2$. The alcohol/ketone ratio was still >1 for $[Fe^{II}(\mathbf{7})_2]OTf_2$ and $[Fe^{II}(\mathbf{8})_2(OTf)_2]$ under these conditions. A high concentration of radicals formed from the peroxides promote free-radical chain mechanisms, which result in low alcohol/ketone ratios.[48] When H_2O_2 is added slowly as a dilute solution, the concentration of free radicals is minimized, and iron-centered $[Fe^{n}{=}O]$ species formed by a reaction of the peroxide with the iron complex might be the actual oxidant[48] through insertion of the oxygen into a C–H bond of the cyclohexane to give cyclohexanol, which results in a high alcohol/ketone ratio (see below). It appears that complex $[Fe^{II}(\mathbf{6})_2]OTf_2$ promotes a mechanistic pathway through an iron–oxo species, as seen from the high alcohol/ketone ratio of 6.6, which is on the same order as reported for iron complexes with tetradentate ligands such as $[Fe^{II}(tpa)(OTf)_2]$.[26]

On the other hand, when *t*BuOOH was employed as the oxidant, the alcohol/ketone ratio was always low (0.5–0.66) and showed barely a change with the *t*BuOOH/cyclohexane ratio or on how the oxidant was added to the reaction mixtures. It has been reported that *t*BuO· radicals readily diffuse and can induce radical chain reactions involving dioxygen, which result in a low alcohol/ketone ratio (see below).[13d]

The alcohol/ketone ratios did not significantly change when the experiments were performed under inert conditions. When the iron complexes were combined with the peroxide oxidants without substrate, we typically observed some heat evolution and occasionally bubbling, which might be evidence for catalase activity, that is, peroxide decomposition to water and oxygen. The systems could create their own oxygen atmosphere under inert conditions, which would explain the outcome of the observed low alcohol/ketone ratios.

Next, we employed complex $[Fe^{II}(\mathbf{6})_2]OTf_2$ in oxidation reactions of activated methylene groups, secondary alcohols, and cyclohexene utilizing *t*BuOOH as the oxidant (Table 5, which also includes the previously reported yields obtained with $[Fe^{II}(\mathbf{4a})_2(OTf_2)]$).[33a]

At a *t*BuOOH/substrate ratio of 4:1 and a catalyst load of 3 mol%, after 4 h at room temperature the corresponding ketone products were obtained in 34 to 85% yield of isolated product. Toluene was oxidized to benzaldehyde in 57% yield and cyclohexene to the corresponding epoxide in 28% yield utilizing similar conditions. Primary alcohols were not oxidized under the conditions in Table 5. Preliminary GC studies showed that the conversions for the other two complexes $[Fe^{II}(\mathbf{7})_2]OTf_2$ and $[Fe^{II}(\mathbf{8})_2(OTf)_2]$ synthesized for this study were comparable. As $[Fe^{II}(\mathbf{6})_2]OTf_2$ is the most easily accessible complex, it was employed for further studies.

The previously synthesized imine complex $[Fe^{II}(\mathbf{4a})_2(OTf)_2]$ gave yields of isolated product between 22 and 91% for the reactions illustrated in Table 5. The yields for the oxidation of "doubly activated" substrates such as diphenylmethane or anthracene were comparable for the two complexes $[Fe^{II}(\mathbf{6})_2]OTf_2$ and $[Fe^{II}(\mathbf{4a})_2(OTf)_2]$. With imine complex $[Fe^{II}(\mathbf{4a})_2(OTf)_2]$ yields of isolated product were lower for the oxidation of secondary alcohols to their corresponding ketones. As opposed to amine complex $[Fe^{II}(\mathbf{6})_2]OTf_2$, imine complex $[Fe^{II}(\mathbf{4a})_2(OTf)_2]$ did not

Table 5. Oxidation reactions employing iron complexes $[Fe^{II}(\mathbf{6})_2]OTf_2$ and $[Fe^{II}(\mathbf{4a})_2(OTf)_2]$ as catalyst and *t*BuOOH as oxidant.

Entry	Substrate (**9**)	Product (**10**)[a]	Yield of $[Fe^{II}(\mathbf{6})_2]^{2+}$ [%][b]	Yield[33a] of $[Fe(\mathbf{4a})_2]^{+}$ [%][b]
1	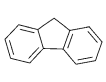	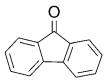	85	91
2	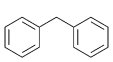	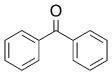	76	74
3	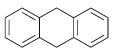	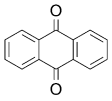	79	51
4			34	47
5			71	22
6	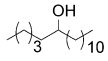	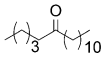	69	–
7			67	47
8			58	23
9			57	–
10			28	–

[a] Typical conditions: Substrate (0.6 mmol), *t*BuOOH (2.4 mmol), and catalyst (3 mol%), 4 h at room temperature in CH_3CN/pyridine (1:1, 2 mL). The products were isolated by using column chromatography. [b] Yield of isolated product.

show catalytic activity at all for the oxidation of toluene or cyclohexene.

To obtain additional information for catalytic efficiencies, we followed the oxidation of diphenylmethane with *t*BuOOH (entry 2 in Table 5) by GC at the significantly reduced catalyst loading of 0.3 mol% over 3 h for all iron complexes $[Fe^{II}(\mathbf{6})_2]OTf_2$, $[Fe^{II}(\mathbf{7})_2]OTf_2$, and $[Fe^{II}(\mathbf{8})_2(OTf)_2]$ utilized for this study. The known complexes $[Fe^{II}(tpa)(OTf)_2]$ and $[Fe^{II}(\mathbf{4a})_2(OTf)_2]$ were also investigated under the same conditions. The traces are compiled in Figure 3, which also displays the observed rate constant k_{obs} for the different catalysts. At this low catalyst loading, it appears that the reactions largely follow a pseudo-zero-order rate law and the k_{obs} values are derived from the slopes of the linear trends. A trace for material "**19**" that was obtained by pretreatment of $[Fe^{II}(\mathbf{6})_2]OTf_2$ with *t*BuOOH is included as well (see below).

As can be seen from Figure 3, the catalytic activity is about comparable for complexes $[Fe^{II}(\mathbf{6})_2]OTf_2$ and $[Fe^{II}(\mathbf{7})_2]OTf_2$ (k_{obs} = 0.19 and 0.1 min^{-1}). It is slightly lower for $[Fe^{II}(tpa)(OTf)_2]$, $[Fe^{II}(\mathbf{4a})_2(OTf)_2]$, and $[Fe^{II}(\mathbf{8})_2(OTf)_2]$ (k_{obs} = 0.045, 0.059, and 0.018 min^{-1}, respectively). Complex $[Fe^{II}(\mathbf{4a})_2(OTf)_2]$ also gave lower yields for some of the oxidation reactions in Table 5, which is in accord with its lower activity than $[Fe^{II}(\mathbf{6})_2]OTf_2$. However, in general, the catalytic activities of the complexes do not differ greatly.

Experiments to better understand the course of the oxidation reactions

The course of iron-catalyzed oxidation reactions with peroxide oxidants is still an objective of current research. A simplified mechanistic picture for ROOH is outlined in Scheme 2 (R = H, *t*Bu).[11a,48,49] It seems to be generally accepted that the reaction of an iron complex with ROOH first yields an iron–peroxo species $[Fe^{III}–O–O–R]$ (**11**), which has been described as not oxidizing organic substrates and is only a precursor of the actual oxidants.[50]

The further course of the oxidation reaction depends on the "fate" of species **11**; it decays by either homolytic or heterolytic bond cleavage of the Fe–O or O–O bond, which has been reported to depend on the spin state of the iron complex[51] and on the pH value.[52] Homolytic cleavage of the O–O or Fe–O bond yields R–O$^{\bullet}$ or H–O$^{\bullet}$ radicals eventually. These radicals can abstract hydrogen atoms from hydrocarbons, which leads to unfavorable radical chain oxidation reactions following a Haber–Weis mechanism (Scheme 2, right-hand path);[11a] O_2 from the atmosphere (or from iron-catalyzed peroxide decomposition) is incorporated through the course of the reaction. The peroxo radical **14** disproportionates through a Russel-type

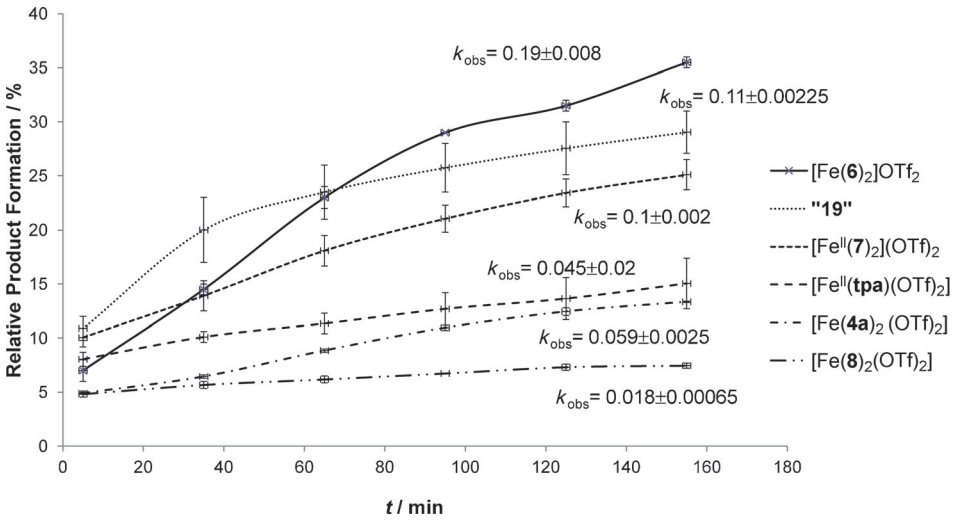

Figure 3. Activity comparison of different iron complexes. The k_{obs} values were determined from the linear trends of the traces, which are not shown.

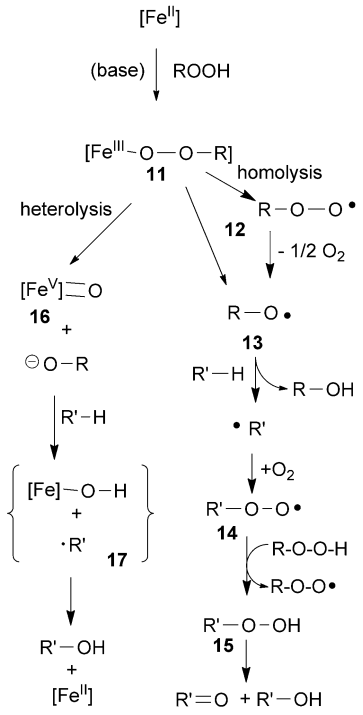

Scheme 2. Simplified reactivities of iron complexes with ROOH (R = H, *t*Bu).

termination[53] and peroxide **15** disproportionates promoted by iron,[54] which gives low alcohol/ketone ratios under alkane oxidations. It has been reported that the reaction can still proceed through an iron-centered oxidant if the concentration of the radicals is kept low by slow addition of the oxidant.[11a,48]

Heterolytic cleavage of iron–peroxo species **11** gives a high-valent iron–oxo species [Fe^{V}=O] (**16**), which is a metal-centered oxidant.[50,55] Its oxidation chemistry is much better controlled through supporting ligands on the iron center, and its existence has been documented for biomimetic, nonheme iron complexes spectroscopically,[56] structurally,[57] and computationally.[58] The [Fe^{V}=O] species can be stabilized by appropriate ligands and can insert an oxygen atom into a C–H bond through a "bound–rebound mechanism"[11a] involving the bracketed intermediate **17** in Scheme 2, in which the radical intermediate R′ presumably never leaves the solvent cage and does not diffuse freely. This pathway gives specifically alcohols as the oxidation products, and [Fe^{II}] is recovered, which can participate in another oxidation cycle.

As outlined above, the catalytic oxidation of cyclohexane utilizing *t*BuOOH appears to proceed through a radical mechanism (as seen by the low alcohol/ketone ratios in Table 4). Only complex [Fe^{II}(**6**)$_2$]OTf$_2$ gives a high alcohol/ketone ratio of 6.6 (Table 4), when H_2O_2 is employed as the oxidant; this reaction presumably involves the iron-centered oxidant **16** (Scheme 2). Notably, complex [Fe^{II}(**6**)$_2$]OTf$_2$ exhibits an N–H unit; it may become significantly acidic upon coordination to the iron center. A nonradical reaction pathway through an iron–oxo species might be promoted at low pH values.[52] Furthermore, for complex [Fe^{II}(**6**)$_2$]OTf$_2$, the alcohol/ketone ratio does not significantly change when performed in the presence of 2,4,6-tri-*tert*-butylphenol (TBPH), which is an efficient scavenger for oxygen-centered radicals.[59]

It is largely accepted that iron-catalyzed oxidations with *t*BuOOH follow a radical mechanism.[13d] Still, the oxidation reactions in Table 5 do not proceed without a catalyst. Only an 8% conversion of diphenylmethane to benzophenone was observed when the radical initiator azobisisobutyronitrile (AIBN) was employed in place of the catalyst at a significantly higher reaction temperature of 80 °C [Eq. (1)]. The iron complexes might, thus, provide a steady supply of *t*BuO• radicals in solution to keep the reaction running.

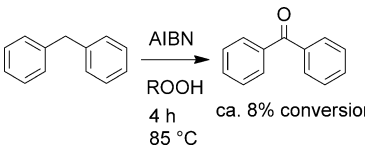

(1)

In the oxidation of benzylic methylene groups, such as fluorene or diphenylmethane (entries 1 to 5 in Table 5), we never observed alcohol products. The oxidation reactions are not retarded or inhibited by the radical scavenger TBPH. However, it has been our observation that benzylic alcohols such as 1-phenylethanol are easily oxidized by peroxides under the reaction conditions, even without a catalyst. Thus, it is not possible to establish an alcohol/ketone ratio to elucidate a mechanism. It appears reasonable to assume that the activated methylene groups in Table 5 are oxidized first to the alcohol. Alcohols are in general more easily oxidized[15] and could, under the reaction conditions, be further oxidized rapidly to the ketone (Scheme 3, top).

To corroborate the faster oxidation of alcohols relative to benzylic methylene groups, we performed a competition experiment between an alcohol and a hydrocarbon (Scheme 3, bottom). When a 1:1 mixture of diphenylmethane and cyclooctanol was treated with 0.5 equivalents *t*BuOOH under conditions identical to those in Table 5, 43% of the cyclooctanol but only 11% of the diphenylmethane was converted into the corresponding ketone, thereby establishing that the alcohol reacts faster than the benzylic CH_2 unit.

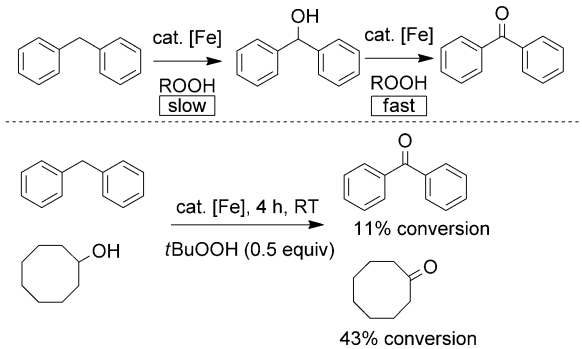

Scheme 3. Potential oxidation sequences (top) and the competition experiment.

The oxidation of the benzylic alcohol intermediates as well as the alcohol substrates in Table 5 to the ketones might proceed through different mechanisms; in the present context, a radical mechanism[60] or a cyclic transition state are potential pathways.[48] In a cyclic transition state the alcohol coordinates first to the iron center as does the peroxide oxidant [Eq. (2)].[48] Intramolecular hydride abstraction from the alcohol by the peroxide might proceed through six-membered transition state **18** [Eq. (2)]; such a transition state is not possible for saturated hydrocarbons, as they typically do not coordinate to a metal center.[48]

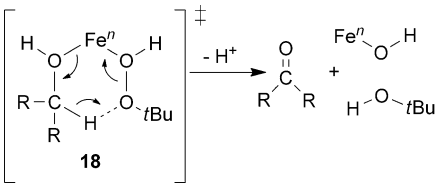

(2)

Alternatively, the oxidation can proceed through a radical mechanism following the pathway depicted in Scheme 2 (right path). Benzylic C–H bonds and C–H bonds in alcohols are weaker than saturated C–H bonds by about 10 kcal mol^{-1}, which explains why the oxidation of alcohols to ketones is much faster than the oxidation of alkanes to alcohols (Scheme 3).[60a] The reactions in Table 5 are not affected by a radical scavenger. However, it has been suggested that iron-catalyzed oxidation reactions can follow several mechanistic pathways simultaneously,[29a,61] and a radical scavenger might block just one of them.

Irrespective of the exact mechanism, a common first intermediate for the title reactions is most likely the iron–peroxo species [Fe^{III}–O–O–R] (**11**, R = H, *t*Bu; Scheme 2). It can be observed by UV/Visible spectroscopy, and has been reported to give a charge-transfer band between $\lambda = 550$ and 630 nm.[28,50,62,63] We hypothesized that UV-spectroscopic monitoring of the formation and decay of the peroxo species [Fe^{III}–O–O–R] could give further information about the catalytic activity of the iron complexes investigated in this study. Accordingly, we recorded UV/Visible spectra over time after treatment of solutions of the complexes in CH_3CN with the peroxide oxidants ROOH in the presence of cyclohexane.

The benzylated amine complex [Fe^{II}(**7**)$_2$]OTf$_2$ gave, immediately after addition of H_2O_2, a new, weak shoulder around 480 nm (Figure 4, top), which slowly decayed over the course of 5 min. Complex [Fe^{II}(**8**)$_2$(OTf)$_2$] gave, immediately after addition of H_2O_2, a new band at $\lambda = 424$ nm with a molar absorption around 700 $M^{-1}cm^{-1}$, which barely changed over time (Figure 4, bottom). The new bands originate presumably—owing to their intensity—from charge transfer. For both complexes, almost identical results were obtained when *t*BuOOH was used as the oxidant (for spectra, see the Supporting Information). The wavelength of the new bands for both complexes are somewhat low for an iron–peroxo complex [Fe–O–O–R], although some complexes have been reported to give charge-transfer bands around 450 nm for that species.[17b] A peroxo species might, under the conditions shown in Figure 4, be very unstable, and the observed bands could also very well be due to intermediates resulting from oxidative ligand decomposition (see below). Still, the fast spectral changes within minutes after addition of an oxidant demonstrate a high reactivity of the two complexes towards the peroxide oxidants.

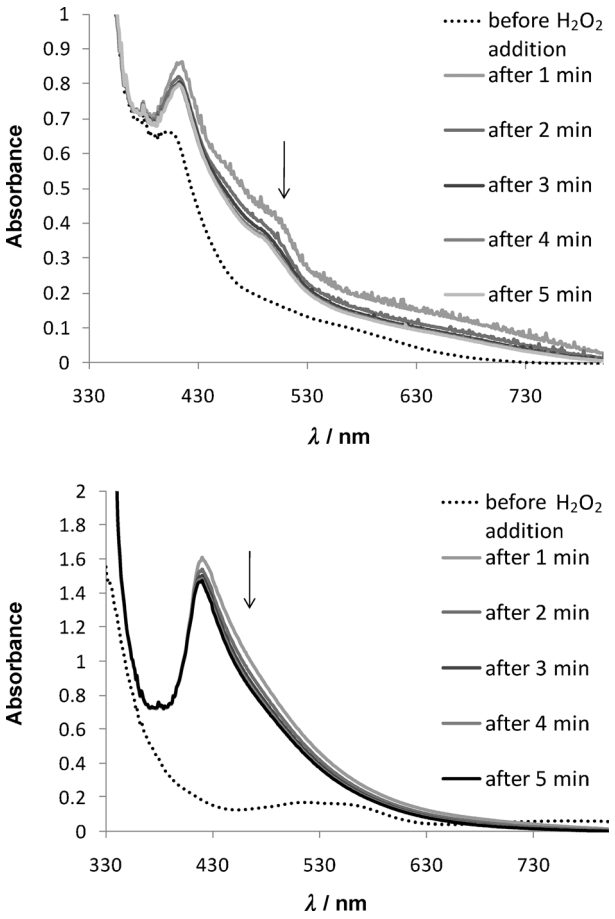

Figure 4. Time-resolved UV/Visible spectra of [Fe(**7**)$_2$]OTf$_2$ (top) and [Fe(**8**)$_2$(OTf)$_2$] (bottom) in CH_3CN after addition of H_2O_2 (dotted line: before addition).

However, the bpa complex [Fe^{II}(**6**)$_2$]OTf$_2$ underwent significant spectroscopic changes in solution when H_2O_2 or *t*BuOOH was added to the complex and UV/Visible spectra were recorded before and immediately after addition of the peroxide in time intervals of one minute. As shown in Figure 5 (top), the intense charge-transfer band for the complex at 434 nm (dotted line) completely disappeared immediately after H_2O_2 was added to the complex. Instead, two new bands formed at 490 and 572 nm. The latter band is characteristic for iron–peroxo species [Fe–OOH] and its molar absorptivity ε (4000 $M^{-1}cm^{-1}$) is also on the same order as previously reported for similar complexes.[28,50,62] This band decayed over a period of 6 min and had completely disappeared after 15 min. When *t*BuOOH was employed, after one minute a new band was observed at 579 nm (ε around 700 $M^{-1}cm^{-1}$, solid line in Figure 5, bottom). The band showed a lower absorptivi-

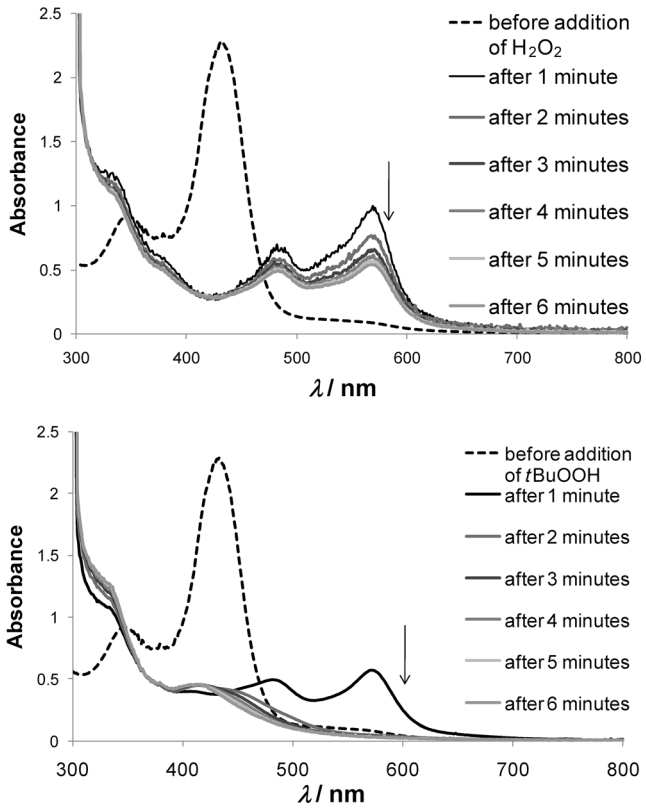

Figure 5. Time-resolved UV/Visible spectra of $[Fe(\mathbf{6})_2]OTf_2$ in CH_3CN after addition of H_2O_2 (top) and *t*BuOOH (bottom). Dotted lines: before addition.

ty than the band obtained with H_2O_2 and had disappeared completely after two minutes.

For $[Fe^{II}(tpa)]^{2+}$, a similar reactivity has been reported previously with *t*BuOOH[62a] and H_2O_2.[50] Upon reaction of the oxidant at −36 °C, a new band at 600 nm ($\varepsilon = 2000\ M^{-1}\,cm^{-1}$) was observed, which was assigned to an iron–peroxo species [Fe–OOH] and that also decayed over time to give a $[Fe^{IV}{=}O]$ species.

However, the transient species that formed in the experiments in Figure 5 cannot be unambiguously assigned to a structure. The spectra in Figure 5 were recorded at room temperature. The new bands around 572 nm are in the range for other [Fe–OOR] species reported in the literature, but these species are typically investigated at much lower temperatures, although studies at room temperature were also reported.[62c] Furthermore, $[Fe(\mathbf{6})_2]OTf_2$ does not immediately have an open coordination site available. It might be that the complex opens a coordination site and forms a peroxo species, but the spectral changes observed over time might also be due to ligand decomposition.

A different behavior was observed for the iron–imine complex $[Fe^{II}(\mathbf{4c})_2(OTf)_2]$, for which an experiment similar to those in Figures 4 and 5 was performed with *t*BuOOH (Figure 6).[33a] After addition of the *t*BuOOH oxidant, the charge-transfer band of the complex at 418 nm intensified, presumably owing to the fact that the polarity of the solution increased after the addition of the aqueous solution of the oxidant. Over the course of 10 min, the charge-transfer band at 418 nm decayed

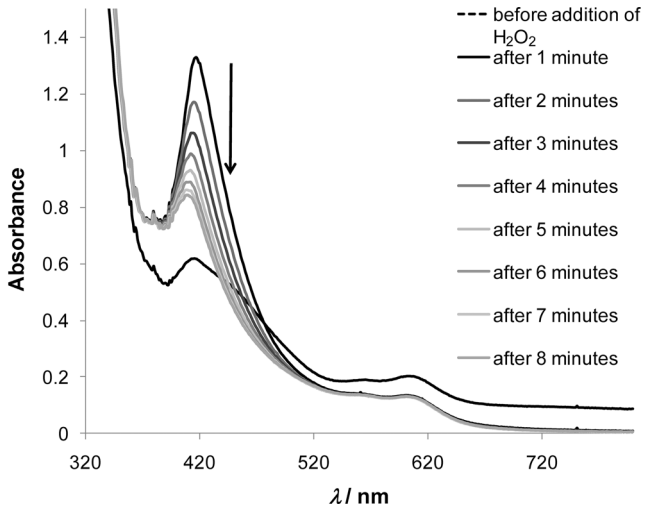

Figure 6. Time-resolved UV/Visible spectra of $[Fe^{II}(\mathbf{4c})_2(OTf_2)]$ in CH_3CN after addition of H_2O_2 (dotted line: before addition).

only very slowly, as opposed to the corresponding bands for $[Fe^{II}(\mathbf{6})_2]OTf_2$, which had completely decayed two minutes after the addition of the oxidant (Figure 5). A band around 600 nm was not observed for $[Fe^{II}(\mathbf{4c})_2(OTf)_2]$. The slow decay of the band at 418 nm could indicate slow ligand decomposition, as imines are somewhat more difficult to oxidize than amines.

Ligand-decomposition pathways and their impact on the catalytic activity

As demonstrated in the previous sections, different ligand architectures can have an impact on the catalytic activity of their respective metal complexes. It has been argued that oxidative ligand decomposition during catalytic applications can decrease the catalytic activity of metal complexes,[64] although the opposite has been reported for pyridin-2-yl-type ligands and their manganese complexes.[65] We were, thus, interested in determining what decomposition products are formed as a consequence of ligand oxidation under catalytic conditions from the iron complexes investigated in this study and how the oxidation of the ligands impairs the catalytic activity.

Accordingly, the $[Fe^{II}(\mathbf{6})_2]OTf_2$ complex was treated with *t*BuOOH under catalytic conditions identical to those employed in the reactions shown in Table 5 but without the presence of substrate. The oxidative decomposition products of the iron complex were isolated as a mixture, which was complex and could not be analyzed by NMR spectroscopy or MS [although a species bearing two oxidized ligands was identified by MS; Eq. (3)]. The mixture will be referred to subsequently as "**19**".

We were, thus, looking for a method to detach the ligands from the iron center after oxidation to identify ligand-decomposition products. Accordingly, $[Fe^{II}(\mathbf{6})_2]OTf_2$ was treated with *t*BuOOH under conditions otherwise identical to the catalysis experiment shown in Table 5, but without a substrate. The ligands were subsequently displaced from the iron center by adding aqueous NaCN to the reaction mixture. The displaced ligands (or their oxidation products, respectively) were isolated

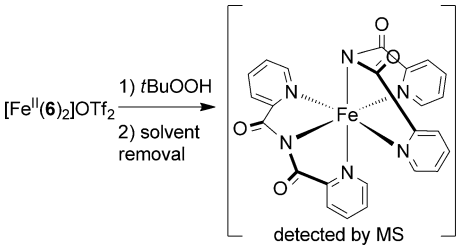

(3)

by extraction and analyzed by GC–MS, NMR spectroscopy, and IR spectroscopy. Similar reactions were performed with the other complexes [Fe^{II}(tpa)(OTf)$_2$], [Fe^{II}(**7**)$_2$]OTf$_2$, and [Fe^{II}(**4a**)$_2$-(OTf)$_2$], in which the material obtained was analyzed by GC–MS. The results are compiled in Scheme 4, and the GC–MS traces are given in the Supporting Information. In all cases, about 90% of the expected mass was recovered, and, thus, little material was lost during workup.

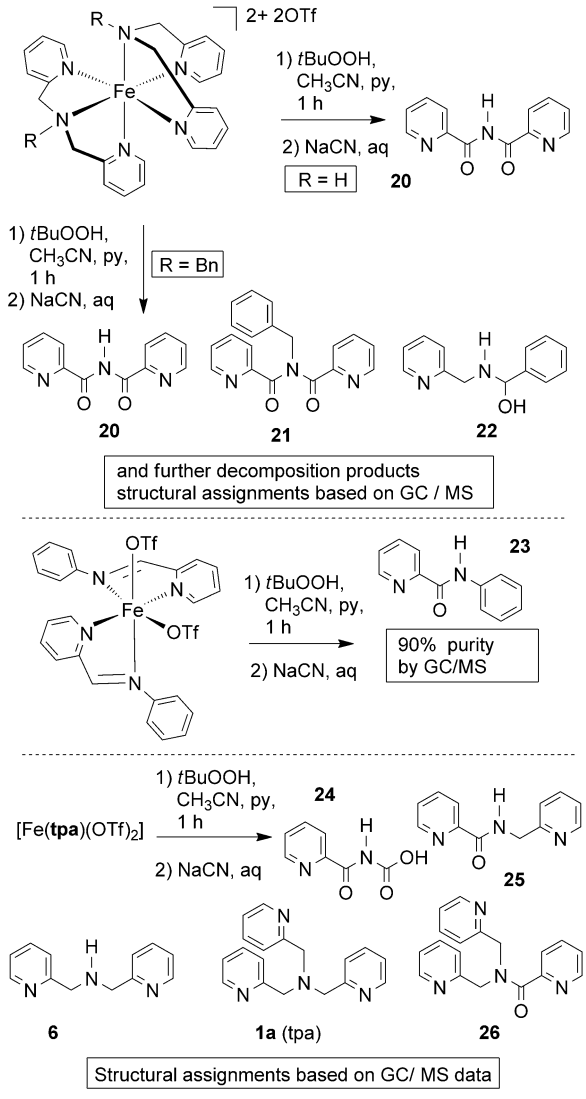

Scheme 4. Experiments to determine ligand-decomposition products under oxidative conditions.

Ligands **6** in [Fe^{II}(**6**)$_2$]OTf$_2$ were cleanly oxidized to the corresponding diamide **20**, which was the only product detected after isolation. For [Fe^{II}(**7**)$_2$]OTf$_2$, a complex mixture of decomposition products was observed, and only the three major components are displayed in Scheme 4. Diamide **20** was detected, together with some **21** and **22**; the benzyl or picolyl units can be oxidatively cleaved from the ligands after oxidation of the CH_2 units, as observed previously in copper complexes bearing structurally related ligands.[66] The imine unit in [Fe^{II}(**4a**)$_2$(OTf)$_2$] also was oxidized cleanly to the corresponding amide **23**. Complex [Fe^{II}(tpa)(OTf)$_2$] behaves slightly differently; it was only oxidized partially to compounds **6**, **24**, **25**, and **26**, and the material isolated after oxidation also contained the original tpa ligand **1a**.

It appeared that the NCH_2 unit of the ligands is commonly oxidized to an amide NC=O for the three complexes, presumably through an intramolecular oxygen transfer from an Fe=O species **27** (Scheme 5), as previously suggested for an intramo-

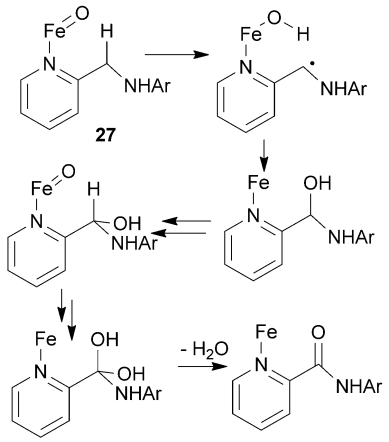

Scheme 5. Potential pathway for an intramolecular NHC_2 oxidation.

lecular aryl hydroxylation reaction involving the iron complex [Fe^{II}(**L**)(CH_3CN)$_2$](ClO_4)$_2$ (**L** = modified tpa).[67] Copper[68] and iron[69] complexes of diamide **20** are known; in all these cases, the amide ligands are coordinated through the N atoms to the iron center, as shown by X-ray studies. Related iron–amide complexes are still capable of catalytically activating H_2O_2.[70] Thus, it is likely that the decomposed ligands in Scheme 4 were still coordinated to the iron, after they had been oxidized to the corresponding amides.

Interestingly, we did not observe any chemical changes of the aryl or pyridyl ring systems of the ligands (although small amounts of bipyridine were sometimes detected, which might have resulted from oxidative dimerization of the pyridine solvent). When iron complex [Fe^{II}(**6**)$_2$]OTf$_2$ was subjected to ligand displacement without prior exposure to the *t*BuOOH oxidant, only the unoxidized ligand **6** was recovered. Thus, the oxidation of the ligand does not take place during the displacement procedure.

We were finally interested to determine whether or not the oxidized ligands could impair the catalytic selectivity and activ-

ity, and material "**19**" was employed for that purpose, which was obtained by oxidizing $[Fe^{II}(\mathbf{6})_2]OTf_2$ utilizing *t*BuOOH as described above [Eq. (3)]. Material "**19**" was subsequently employed in the determination of the catalytic activity in the oxidation of diphenylmethane in the same way as it was performed for the unoxidized iron complexes in Figure 3. Somewhat surprisingly, the catalytic activity of "**19**" is comparable to the unoxidized complex $[Fe^{II}(\mathbf{6})_2]OTf_2$ (Figure 3, $k_{obs} = 0.11$). However, the exact composition of the isolated oxidized material "**19**" is not known, thus making a direct comparison of absolute values difficult.

Likewise, when oxidized material "**19**" was employed in the cyclohexane oxidations in Table 4, the alcohol/ketone ratio decreased, relative to the unoxidized complex $[Fe^{II}(\mathbf{6})_2]OTf_2$, from 6.6 to 3. The selectivity of "**19**" is somewhat lower than that of its precursor, but still higher than those of the other complexes synthesized for this study. Thus, oxidative ligand decomposition slightly decreases the selectivity of the complex in the oxidation of cyclohexane but has no measurable negative impact on the catalytic activity for the oxidation of diphenylmethane under the conditions in Figure 3.

The catalytic activity of "**19**", which was obtained by oxidation of $[Fe^{II}(\mathbf{6})_2]OTf_2$ [Eq. (3)] shows catalytic activity in the test reaction for Figure 3 that is comparable to the other complexes. The ligand-decomposition experiments (Scheme 4) revealed that in the ligands the NCH_2 units are oxidized to the amides NC=O as reported for other iron complexes,[72] but the ligands largely remain di-, tri-, or tetradentate. Consequently, the pyridyl units for the ligands can still coordinate to the iron center through the nitrogen atoms, as shown for related systems,[69,70] even after oxidative degradation of the ligand, which seems to be the major aspect for retaining catalytic activity. It has been described before that in manganese-based catalyst systems the oxidation of pyridyl-based ligands to pyridine-2-carboxylic acid takes place prior to the onset of the catalytic oxidation of organic substrates.[65] In our catalytic systems, the oxidation of the ligand appears to be very fast and our reactions do not exhibit an induction period (Figure 3). Thus, we cannot determine whether or not the oxidation of the ligands is a necessary prerequisite for developing catalytic activity, but oxidation of the ligands, in turn, does not shut down the activity.

Discussion

The preceding data establish that the iron complexes $[Fe^{II}(\mathbf{6})_2]OTf_2$ and $[Fe^{II}(\mathbf{7})_2]OTf_2$ with tridentate aminopyridine ligands are another efficient class of iron catalysts active for the oxidation of CH_2 groups and alcohols to the corresponding ketones with peroxide oxidants. The mild reaction conditions (4 h reaction time at room temperature) make them an attractive starting point for further investigation and optimization effort.

It has been argued that two tridentate ligands in the coordination sphere of iron complexes might decrease the catalytic activity, as all six coordination sites are occupied by the ligands.[43] Indeed, the majority of biomimetic, nonheme iron catalysts bear one ligand with four or five nitrogen or oxygen donor atoms.[1d,16a,17b] However, complexes $[Fe^{II}(\mathbf{6})_2]OTf_2$ and $[Fe^{II}(\mathbf{7})_2]OTf_2$ show catalytic activity that is comparable (even slightly higher) than the previously established complex $[Fe^{II}(tpa)(OTf)_2]$ in the oxidation of diphenylmethane in Figure 3. Complex $[Fe^{II}(\mathbf{6})_2]OTf_2$ needed to detach one of the pyridyl rings to initiate catalytic activity if the reaction proceeds through an iron–peroxo intermediate [Fe–OOR]. However, complex $[Fe^{II}(\mathbf{6})_2]OTf_2$ with two tridentate ligands could also operate through an outer-sphere electron-transfer mechanism,[71] and the species observed in the UV/Visible spectrum is an intermediate of the ligand decomposition that is taking place during the course of the reaction.

Complex $[Fe^{II}(\mathbf{8})_2(OTf)_2]$ with two bidentate ligands **8** exhibits a somewhat diminished catalytic activity, and so does the imine complex $[Fe^{II}(\mathbf{4a})_2(OTf)_2]$; there is a slight dependency of the catalytic activity on the denticity of the ligands coordinated to the iron center, as the complexes with tris- or tetradentate ligands perform slightly better than the complexes bearing bidentate ligands.

Conclusion

In conclusion, we have synthesized a series of complexes of the general formula $[Fe^{II}\mathbf{L}_n]OTf_2$ ($n = 1$, 2) bearing bi- and tridentate aminopyridyl ligands **L**, two of which were structurally characterized. The new complexes showed catalytic activity in the oxidation of benzylic CH_2 groups and secondary alcohols to the corresponding ketones (3% catalyst load, 4 equivalents ROOH, RT, 4 h, 28 to 85% yield of isolated product). The catalytic activity of the new complexes was determined and compared with previously synthesized iron complexes $[Fe^{II}(tpa)(OTf)_2]$ and $[Fe^{II}(iminopyridyl)_2(OTf)_2]$ bearing the tetradentate tris(picolyl)amine (tpa) and bidentate iminopyridyl ligands in their coordination sphere.

The denticity of the ligands has a slight impact on the catalytic activity, as the iron complexes featuring tri- and tetradentate ligands in their coordination sphere performed slightly better than their bidentate counterparts. Ligand-decomposition products were identified that form under the oxidative, catalytic conditions. It appears that primarily NCH_2 units are oxidized to the corresponding amides NC=O. However, the overall denticity of the ligands largely stays intact, and no oxidations of the pyridyl units were observed. When $[Fe^{II}\mathbf{L}_2]OTf_2$ (**L** = di(picolyl)amine) was treated first with peroxide to obtain "oxidized" material, it was determined that its catalytic activity is not diminished appreciably relative to the "unoxidized" starting material.

The findings presented herein can assist in the future design of catalytically active iron complexes for the title reaction; employment of ligands with a high denticity appears to have a beneficial impact on the performance of the complexes, and oxidative ligand decomposition does not inevitably lead to catalyst deactivation.

Experimental Section

General

Chemicals were treated as follows: toluene and diethyl ether distilled from Na/benzophenone; CH_2Cl_2, MeOH, and CH_3CN distilled from CaH_2. $CHCl_3$, silica, pyridine, tri(2-picolyl)amine (tpa, **1a**), bis(2-picolyl)amine (**6**, all Aldrich), and other materials were used as received. Ligand **7**[42] and $[Fe(OTf)_2]$[73] were prepared according to the literature. All reactions were carried out under nitrogen and by employing standard Schlenk techniques, and workups were carried out in the air.

NMR spectra were obtained at room temperature on a Bruker Avance 300 MHz or a Varian Unity Plus 300 MHz instrument at room temperature and were referenced to a residual solvent signal; all assignments are tentative. GC–MS spectra were recorded on a Hewlett Packard GC–MS System Model 5988A. UV/Visible spectra were recorded on Varian Cary 50 Bio spectrophotometer. Exact masses were obtained on a JEOL MStation [JMS-700] mass spectrometer. IR spectra were recorded on a Thermo Nicolet 360 FTIR spectrometer. Elemental analyses were performed by Atlantic Microlab Inc., Norcross, GA, USA. Magnetic moments, ^{19}F NMR spectra, and UV/Visible data are listed in Table 1.

Synthesis

Ligand 8: 2-Pyridine carboxaldehyde (1.0 g, 9.34 mmol) was dissolved in methanol (10 mL), cooled with an ice bath, while 2-methoxyaniline (1.16 g, 9.43 mmol) in methanol (10 mL) was added dropwise. The ice bath was then removed, allowing the reaction to stir for 1 h at room temperature. Then $NaBH_4$ (0.741 g, 19.61 mmol) was added in 3 portions at 0 °C. The reaction mixture was then allowed to stir overnight at room temperature. After 12 h, aqueous HCl solution (5 M) was added until a pH of 4 was reached. The reaction mixture was then allowed to stir at room temperature for an additional hour. Then aqueous NaOH (2 M) solution was added until a pH of 12 was reached. Then CH_2Cl_2 (30 mL) was added and the two layers were transferred to a separating funnel. The organic phase was collected and the product was extracted from the aqueous layer, using CH_2Cl_2 (2×30 mL). The combined organic layers were dried over sodium sulfate and the solvent was removed under vacuum to yield a yellow oil that was subsequently purified by means of column chromatography (CH_2Cl_2/Et_3N 90:10 as eluent) to give ligand **8** as a red oil (1.87 g, 8.73 mmol, 94%). ^1H NMR (300 MHz, $CDCl_3$, 25 °C, TMS): $\delta = 8.55$ (d, J(H,H) = 2.9 Hz, 1H; pyridyl–H), 7.53 (t, J(H,H) = 6.7 Hz, 1H; pyridyl–H), 7.28 (d, J(H,H) = 7.2 Hz, 1H; pyridyl–H), 7.10 (d, J(H,H) = 7.2 Hz, 1H; pyridyl–H), 6.82–6.75 (m, 2H; Ar–H), 6.67–6.62 (m, 1H; Ar–H), 6.51 (d, J(H,H) = 7.6 Hz, 1H; Ar–H), 5.19 (s, 1H; NH), 4.45 (s, 2H; CH_2), 3.82 ppm (s, 3H; OCH_3); $^{13}C\{^1H\}$ NMR (300 MHz, $CDCl_3$, 25 °C, TMS): $\delta = 159.5$ (s; aromatic), 149.6 (s; aromatic), 147.4 (s; aromatic), 138.2 (s; aromatic), 137.1 (aromatic), 122.4 (s; aromatic), 121.8 (s; aromatic), 117.2 (s; aromatic), 110.6 (s; aromatic). 109.9 (s; aromatic), 55.8 (s; NCH_2), 49.6 ppm (s; OCH_3); IR (neat oil): $\tilde{\nu} = 3391$ cm^{-1} (m, NH); MS (FAB): m/z (%): 214 (100) [**8**$^+$].

[Fe(6)$_2$]OTf$_2$: Acetonitrile (3 mL) was added to a Schlenk flask containing $[Fe(OTf)_2]$ (0.211 g, 0.483 mmol). Ligand **6** (0.192 g, 0.967 mmol) was added to the resulting yellow transparent solution and the resulting red solution was allowed to stir for 30 min at room temperature. This mixture was then concentrated to about 1 mL, cooled down to 0 °C, layered with diethyl ether (10 mL), and stored at −18 °C overnight to yield a red crystalline precipitate. The supernatant was decanted and the precipitate was dried under high vacuum to give $[Fe(\mathbf{6})_2]OTf_2$ as red crystals (0.351 g, 0.466 mmol, 96%). ^1H NMR (300 MHz, CD_3CN, 25 °C, TMS): $\delta = 9.12$ (brs, 4H; pyridyl–H), 7.97 (brs, 2H; pyridyl–H), 7.82 (t, J(H,H) = 7.2 Hz, 8H; pyridyl–H), 7.64 (brs, 2H; pyridyl–H), 5.95 (s, 2H; NH), 5.36–5.25 ppm (m, 8H; 4CH_2); ^1H NMR (300 MHz, [D_6]acetone, −50 °C, TMS): $\delta = 9.11$ (d, ^2J(H,H) = 5.0 Hz, 2H; NCH pyridyl), 8.29 (d, ^2J(H,H) = 5.0 Hz, 2H; NCH, pyridyl), 7.93 (t, ^3J(H,H) = 7.3 Hz, 2H; pyridyl), 7.79 (t, ^3J(H,H) = 7.3 Hz, 2H; pyridyl), 7.71 (d, ^2J(H,H) = 7.4 Hz, 4H; pyridyl), 7.29 (t, ^3J(H,H) = 6.0 Hz, 2H; pyridyl), 6.05 (s, 2H; NH), 5.19 (dd, ^2J(H,H) = 8.4 Hz, 2H; NC*H*H′), 4.44 (d, ^2J(H,H) = 16.5 Hz, 2H; NC*H*H′), 4.35 (d, ^2J(H,H) = 18.5 Hz, 2H; NCH*H*′), 4.27 ppm (d, ^2J(H,H) = 11.5 Hz, 2H; NCH*H*′); $^{13}C\{^1H\}$ NMR (75 MHz, [D_6]acetone, 25 °C, TMS): $\delta = 164.4$ (pyridyl), 156.0 (pyridyl), 137.8 (pyridyl), 128.5 (pyridyl), 124.3 (pyridyl), 59.0 ppm (CH_2); IR (neat solid): $\tilde{\nu} = 3245$ (m, N–H), 1254 (s, OTf), 1162 (sh, OTf), 1028 cm^{-1} (sh, OTf); MS (FAB): m/z (%): 603 (30) [Fe(**6**)$_2$OTf$^+$], 404 (100) [Fe(**6**)OTf$^+$], 255 (20) [Fe(**6**)$^+$]; HRMS: m/z calcd for $C_{25}H_{26}F_3{}^{56}FeN_6O_3S$: 603.10883; found: 603.1091 (corresponds to [Fe(**6**)$_2$(OTf)]$^+$); elemental analysis calcd (%) for $C_{26}H_{26}F_6FeN_6O_6S_2$: C 41.50, H 3.48, found: C 41.64, H 3.49.

[Fe(7)$_2$]OTf$_2$: Acetonitrile (2 mL) was added to a Schlenk flask containing benzylbis(2-picolyl)amine (**7**, 0.082 g, 0.283 mmol). Subsequently, $[Fe(OTf)_2]$ (0.062 g, 0.141 mmol) was added to the red-orange solution. The red-orange solution was then heated at 60 °C for 1 h. The resulting solution was cooled down to 0 °C and layered with diethyl ether (8 mL) and stored at −18 °C overnight to yield a red-tan precipitate. The supernatant was decanted and the resulting solid was washed with cold diethyl ether (3×5 mL) and dried under high vacuum to give the product $[Fe(\mathbf{7})_2]OTf_2$ as a red-tan solid (0.119 g, 0.128 mmol, 90%). ^1H NMR (300 MHz, CD_3CN, 25 °C, TMS): $\delta = 111.6$ (brs, 2H; pyridyl–H), 75.9 (brs, 2H; pyridyl–H), 64.6 (brs, 2H; pyridyl–H), 58.0 (brs, 2H; pyridyl–H), 44.5 (brs, 2H; pyridyl–H), 42.5 (brs, 2H; pyridyl–H), 41.3 (brs, 2H; pyridyl–H), 15.4 (s, 3H), 13.7 (s, 3H), 8.36 (brs, 2H), 7.36 (brs, 4H), 6.20 (brs, 2H), 4.81–4.17 (m, 4H), 3.39 (s, 1H), 1.99 (s, 1H), −10.2 (s, 1H; pyridyl–H), −16.4 (s, 1H; pyridyl–H), −19.0 ppm (s, 2H; pyridyl–H); IR (neat solid) $\tilde{\nu} = 1251$ (s, OTf), 1152 (m, OTf), 1028 cm^{-1} (s-sh, OTf); MS (FAB): m/z (%): 783 (30) [Fe(**7**)$_2$(OTf)]$^+$, 494 (100) [Fe(**7**)(OTf)]$^+$; HRMS: m/z calcd for $C_{39}H_{38}F_3{}^{56}FeN_6O_3S$: 783.20270; found: 783.2018 (corresponds to [Fe(**7**)$_2$(OTf)]$^+$); elemental analysis calcd (%) for $C_{40}H_{38}F_6FeN_6O_6S_2$: C 51.51, H 4.11; found: C 50.68, H 4.07.

[Fe(8)$_2$(OTf)$_2$]: Acetonitrile (3 mL) was added to a Schlenk flask containing $[Fe(OTf)_2]$ (0.265 g, 0.607 mmol). Ligand **8** (0.260 g, 1.22 mmol) was added to the yellow transparent solution and the resulting red-purple solution was allowed to stir for 1.5 h at room temperature. This mixture was then concentrated to about 1.5 mL, cooled down to 0 °C, layered with diethyl ether (10 mL), and stored at −18 °C overnight to yield a purple crystalline precipitate. The supernatant was decanted and the precipitate was dried under high vacuum to give $[Fe(\mathbf{8})_2(OTf)_2]$ as purple crystals (0.443 g, 0.566 mmol, 93%). ^1H NMR (300 MHz, CD_3CN, 25 °C, TMS): $\delta = 53.9$ (brs, 2H; pyridyl–H), 45.3 (brs, 2H; pyridyl–H), 11.9 (brs, 2H; pyridyl–H), 6.6–4.4 (brs, ca. 18H), −20.8 ppm (s, 2H; pyridyl–H); IR (neat solid): $\tilde{\nu} = 3268$ (w, N–H), 1239 (s, OTf), 1157 (m, OTf), 1024 cm^{-1} (s sh, OTf); MS (FAB): m/z (%): 633 (30) [Fe(**8**)$_2$(OTf)$^+$], 419 (100) [Fe(**8**)(OTf)$^+$]; HRMS: m/z calcd for $C_{27}H_{28}F_3{}^{56}FeN_4O_5S$: 633.10809; found: 633.1081 (corresponds to [Fe(**8**)$_2$(OTf)]$^+$); elemental analysis calcd (%) for $C_{28}H_{28}F_6FeN_4O_8S_2$: C 42.98, H 3.61; found: C 42.57, H 3.74.

Representative catalytic procedure (Table 5)

The substrate fluorene (0.100 g, 0.601 mmol) and the catalyst $[Fe^{II}(\mathbf{6})_2]OTf_2$ (0.014 g, 0.018 mmol) were dissolved in pyridine (1.0 mL) and CH_3CN (1.0 mL). The oxidant *t*BuOOH (0.344 mL, 70 wt% in H_2O, 2.4 mmol) was added dropwise and the tan solution was shaken for 5 h at room temperature. The pyridine and CH_3CN solvents were removed under vacuum. The product fluorenone was isolated by column chromatography as a colorless oil (0.092 g, 0.510 mmol, 85%) using silica gel and $CHCl_3$ as eluent. Spectroscopic data and copies of the ^1H and $^{13}C\{^1H\}$ NMR spectra of all catalysis products in Table 5 are given in the Supporting Information.

X-ray crystal structure determinations of $[Fe(6)_2]OTf_2$ and $[Fe(8)_2(OTf)_2]$

Suitable crystals of appropriate dimensions were mounted on Mitgen loops in random orientations. Preliminary examination and data collection were performed using a Bruker Kappa Apex-II charge-coupled device (CCD) detector system single-crystal X-ray diffractometer equipped with an Oxford Cryostream LT device. Data were collected using graphite-monochromated $Mo_{K\alpha}$ radiation ($\lambda = 0.71073$ Å) from a fine-focus sealed-tube X-ray source. Preliminary unit-cell constants were determined with a set of 36 narrow frame scans. Typical data sets consist of combinations of ω and ϕ scan frames with a typical scan width of 0.5° and counting time of 15–30 s/frame at a crystal to detector distance of approximately 3.5 to 4.0 cm. The collected frames were integrated using an orientation matrix determined from the narrow frame scans. Apex II and SAINT software packages[74] were used for data collection and data integration. Analysis of the integrated data did not show any decay. Final cell constants were determined by global refinement of reflections from the complete data set. Data were corrected for systematic errors using SADABS[74] based on the Laue symmetry using equivalent reflections. Structure solutions and refinement were carried out using the SHELXTL-PLUS software package.[75] The structures were refined with full-matrix least-squares cycles by minimizing $\Sigma w(F_o^2 - F_c^2)^2$. All non-hydrogen atoms were refined anisotropically to convergence. Typically, H atoms were added at the calculated positions in the final refinement cycles. Specific details of refinement for the compounds are listed below.

$[Fe(\mathbf{6})_2]OTf_2$ was refined as a twin in the space group P_n with BASF refining to 0.669. Some of the CF_3 and SO_3 groups of the anion are disordered. The disorder was modeled with partial occupancy atoms and refined with restraints. The NH hydrogen atoms were located and refined with a riding model. The structure can be solved and refined in *P*2/*n* but this results in poor refinement and geometry.

$[Fe(\mathbf{8})_2(OTf)_2]$ was refined in the space group $P\bar{1}$. The coordinated CF_3SO_3 group is disordered. The disorder was modeled with partial occupancy atoms and refined with restraints. The NH hydrogen atoms were located and refined with a riding model.

CCDC-852959 ($[Fe^{II}(\mathbf{6})_2]OTf_2$) and 852960 ($[Fe^{II}(\mathbf{8})_2(OTf)_2]$) contains the supplementary crystallographic data for this paper. These data can be obtained free of charge from The Cambridge Crystallographic Data Centre via www.ccdc.cam.ac.uk/data_request/cif.

Acknowledgements

Funding from the National Science Foundation for the purchase of the NMR spectrometer (CHE-9974801), the purchase of the ApexII diffractometer (MRI, CHE-0420497), and the purchase of the mass spectrometer (CHE-9708640) is acknowledged.

Keywords: biomimetic catalysis · homogeneous catalysis · ligand effects · N ligands · oxidation

[1] a) C.-L. Sun, B.-J. Li, Z.-J. Shi, *Chem. Rev.* **2011**, *111*, 1293 – 1314; b) W. M. Czaplik, M. Mayer, J. Cvengroš, A. Jacobi von Wangelin, *ChemSusChem* **2009**, *2*, 396 – 417; c) A. A. O. Sarhan, C. Bolm, *Chem. Soc. Rev.* **2009**, *38*, 2730 – 2744; d) E. B. Bauer, *Curr. Org. Chem.* **2008**, *12*, 1341 – 1369; e) S. Enthaler, K. Junge, M. Beller, *Angew. Chem.* **2008**, *120*, 3363 – 3367; *Angew. Chem. Int. Ed.* **2008**, *47*, 3317 – 3321; f) A. Correa, O. Garcia Mancheño, C. Bolm, *Chem. Soc. Rev.* **2008**, *37*, 1108 – 1117; g) B. D. Sherry, A. Fürstner, *Acc. Chem. Res.* **2008**, *41*, 1500 – 1511; h) C. Bolm, J. Legros, J. Le Paih, L. Zani, *Chem. Rev.* **2004**, *104*, 6217 – 6254.

[2] a) M. Lin, X.-l. Chen, T. Wang, P. Yan, S.-x. Xu, Z.-p. Zhan, *Chem. Lett.* **2011**, *40*, 111 – 113; b) G. C. Midya, S. Paladhi, K. Dhara, J. Dash, *Chem. Commun.* **2011**, *47*, 6698 – 6700; c) M. Mayer, W. M. Czaplik, A. Jacobi von Wangelin, *Adv. Synth. Catal.* **2010**, *352*, 2147 – 2152; d) T. Hata, S. Iwata, S. Seto, H. Urabe, *Adv. Synth. Catal.* **2012**, *354*, 1885 – 1889; e) S. Gülak, A. Jacobi von Wangelin, *Angew. Chem.* **2012**, *124*, 1386 – 1390; *Angew. Chem. Int. Ed.* **2012**, *51*, 1357 – 1361.

[3] J. Bonnamour, C. Bolm, *Org. Lett.* **2011**, *13*, 2012 – 2014.

[4] W. Han, P. Mayer, A. R. Ofial, *Adv. Synth. Catal.* **2010**, *352*, 1667 – 1676.

[5] O. G. Mancheno, J. Dallimore, A. Plant, C. Bolm, *Org. Lett.* **2009**, *11*, 2429 – 2432.

[6] a) A. Berkessel, S. Reichau, A. von der Höh, N. Leconte, J.-M. Neudörfl, *Organometallics* **2011**, *30*, 3880 – 3887; b) J. Yang, T. D. Tilley, *Angew. Chem.* **2010**, *122*, 10384 – 10386; *Angew. Chem. Int. Ed.* **2010**, *49*, 10186 – 10188; c) M. Flückiger, A. Togni, *Eur. J. Org. Chem.* **2011**, 4353 – 4360; d) J. M. S. Cardoso, B. Royo, *Chem. Commun.* **2012**, *48*, 4944 – 4946.

[7] A. M. Tondreau, C. Milsmann, A. D. Patrick, H. M. Hoyt, E. Lobkovsky, K. Wieghardt, P. J. Chirik, *J. Am. Chem. Soc.* **2010**, *132*, 15046 – 15059.

[8] a) S. Enthaler, *Eur. J. Org. Chem.* **2011**, *2011*, 4760 – 4763; b) C. Wang, X. Li, F. Wu, B. Wan, *Angew. Chem.* **2011**, *123*, 7300 – 7304; *Angew. Chem. Int. Ed.* **2011**, *50*, 7162 – 7166; c) Y.-Y. Lin, Y.-J. Wang, C.-H. Lin, J.-H. Cheng, C.-F. Lee, *J. Org. Chem.* **2012**, *77*, 6100 – 6106; d) D. Bézier, G. T. Venkanna, L. C. Misal Castro, J. Zheng, T. Roisnel, J.-B. Sortais, C. Darcel, *Adv. Synth. Catal.* **2012**, *354*, 1879 – 1884.

[9] H. J. H. Fenton, *J. Chem. Soc. Trans.* **1894**, *65*, 899 – 910.

[10] a) D. H. R. Barton, *Tetrahedron* **1998**, *54*, 5805 – 5817; b) D. H. R. Barton, *Tetrahedron* **1994**, *50*, 1011 – 1032; c) D. H. R. Barton, D. Doller, *Pure Appl. Chem.* **1991**, *63*, 1567 – 1576; d) D. H. R. Barton, E. Csuhai, D. Doller, N. Ozbalik, G. Balavoine, *Proc. Natl. Acad. Sci. USA* **1990**, *87*, 3401 – 3404.

[11] a) F. Gozzo, *J. Mol. Catal. A* **2001**, *171*, 1 – 22; b) B. Singh, J. R. Long, F. Fabrizia de Biani, D. Gatteschi, P. Stavropoulos, *J. Am. Chem. Soc.* **1997**, *119*, 7030 – 7047.

[12] D. H. R. Barton, *Chem. Soc. Rev.* **1996**, *25*, 237 – 239.

[13] a) P. Stavropoulos, R. Çelenligil-Çetin, A. E. Tapper, *Acc. Chem. Res.* **2001**, *34*, 745 – 752; b) D. W. Snelgrove, P. A. McFaul, K. U. Ingold, D. D. M. Wayner, *Tetrahedron Lett.* **1996**, *37*, 823 – 826; c) M. J. Perkins, *Chem. Soc. Rev.* **1996**, *25*, 229 – 236; d) F. Minisci, F. Fontana, S. Araneo, F. Recupero, S. Banfi, S. Quici, *J. Am. Chem. Soc.* **1995**, *117*, 226 – 232.

[14] E. Neyens, J. Baeyens, *J. Hazard. Mater.* **2003**, *98*, 33 – 50.

[15] P. R. Ortiz de Montellano, *Chem. Rev.* **2010**, *110*, 932 – 948.

[16] a) E. P. Talsi, K. P. Bryliakov, *Coord. Chem. Rev.* **2012**, *256*, 1418 – 1434; b) P. C. A. Bruijnincx, G. van Koten, R. J. M. Klein Gebbink, *Chem. Soc. Rev.* **2008**, *37*, 2716 – 2744.

[17] a) L. Que, Jr., W. B. Tolman, *Nature* **2008**, *455*, 333 – 340; b) M. Costas, M. P. Mehn, M. P. Jensen, L. Que, Jr., *Chem. Rev.* **2004**, *104*, 939 – 986.

[18] a) A. Beck, B. Weibert, N. Burzlaff, *Eur. J. Inorg. Chem.* **2001**, 521 – 527; b) M. Costas, K. Chen, L. Que, Jr., *Coord. Chem. Rev.* **2000**, *200 – 202*, 517 – 544; c) J. T. Groves, *J. Inorg. Biochem.* **2006**, *100*, 434 – 474; d) P. D. Oldenburg, L. Que, Jr., *Catal. Today* **2006**, *117*, 15 – 21; e) N. Burzlaff,

Angew. Chem. **2009**, *121*, 5688 – 5690; *Angew. Chem. Int. Ed.* **2009**, *48*, 5580 – 5582.
[19] B. Join, K. Möller, C. Ziebart, K. Schröder, D. Gördes, K. Thurow, A. Spannenberg, K. Junge, M. Beller, *Adv. Synth. Catal.* **2011**, *353*, 3023 – 3030.
[20] a) A. Company, L. Gómez, X. Fontrodona, X. Ribas, M. Costas, *Chem. Eur. J.* **2008**, *14*, 5727 – 5731; b) J. Tang, P. Gamez, J. Reedijk, *Dalton Trans.* **2007**, 4644 – 4646; c) F. Li, M. Wang, C. Ma, A. Gao, H. Chen, L. Sun, *Dalton Trans.* **2006**, 2427 – 2434.
[21] a) M. Nakanishi, C. Bolm, *Adv. Synth. Catal.* **2007**, *349*, 861 – 864; b) C. Pavan, J. Legros, C. Bolm, *Adv. Synth. Catal.* **2005**, *347*, 703 – 705.
[22] a) R. R. Fernandes, J. Lasri, M. F. C. Guedes da Silva, J. A. L. da Silva, J. J. R. Frausto da Silva, A. J. L. Pombeiro, *J. Mol. Catal. A* **2011**, *351*, 100 – 111; b) S. A. Moyer, T. W. Funk, *Tetrahedron Lett.* **2010**, *51*, 5430 – 5433; c) E. Balogh-Hergovich, G. Speier, *J. Mol. Catal. A* **2005**, *230*, 79 – 83; d) H. Hosseini-Monfared, C. Näther, H. Winkler, C. Janiak, *Inorg. Chim. Acta* **2012**, *391*, 75 – 82.
[23] a) P. Comba, H. Wadepohl, S. Wunderlich, *Eur. J. Inorg. Chem.* **2011**, 5242 – 5249; b) T. M. Shaikha, F.-E. Hong, *Adv. Synth. Catal.* **2011**, *353*, 1491 – 1496.
[24] a) M. Wu, C.-X. Miao, S. Wang, X. Hu, C. Xia, F. E. Kühn, W. Sun, *Adv. Synth. Catal.* **2011**, *353*, 3014 – 3022; b) K. Schröder, B. Join, A. Jose Amali, K. Junge, X. Ribas, M. Costas, M. Beller, *Angew. Chem.* **2011**, *123*, 1461 – 1465; *Angew. Chem. Int. Ed.* **2011**, *50*, 1425 – 1429; c) F. G. Gelalcha, G. Anilkumar, M. K. Tse, A. Brückner, M. Beller, *Chem. Eur. J.* **2008**, *14*, 7687 – 7698; d) P. C. A. Bruijnincx, I. L. C. Buurmans, S. Gosiewska, M. A. H. Moelands, M. Lutz, A. L. Spek, G. van Koten, R. J. M. Klein Gebbink, *Chem. Eur. J.* **2008**, *14*, 1228 – 1237; e) F. Oddon, E. Girgenti, C. Lebrun, C. Marchi-Delapierre, J. Pécaut, S. Ménage, *Eur. J. Inorg. Chem.* **2012**, 85 – 96.
[25] a) M. S. Chen, M. C. White, *Science* **2007**, *318*, 783 – 787; b) M. S. Chen, M. C. White, *Science* **2010**, *327*, 566 – 571.
[26] K. Chen, M. Costas, L. Que, Jr., *J. Chem. Soc. Dalton Trans.* **2002**, 672 – 679.
[27] a) J. England, R. Gondhia, L. Bigorra-Lopez, A. R. Petersen, A. J. P. White, G. J. P. Britovsek, *Dalton Trans.* **2009**, 5319 – 5334; b) J. England, C. R. Davies, M. Banaru, A. J. P. White, G. J. P. Britovsek, *Adv. Synth. Catal.* **2008**, *350*, 883 – 897; c) G. J. P. Britovsek, J. England, A. J. P. White, *Dalton Trans.* **2006**, 1399 – 1408; d) G. J. P. Britovsek, J. England, A. J. P. White, *Inorg. Chem.* **2005**, *44*, 8125 – 8134; e) G. J. P. Britovsek, J. England, S. K. Spitzmesser, A. J. P. White, D. J. Williams, *Dalton Trans.* **2005**, 945 – 955.
[28] S. Gosiewska, H. P. Permentier, A. P. Bruins, G. van Koten, R. J. M. Klein Gebbink, *Dalton Trans.* **2007**, 3365 – 3368.
[29] a) P. Comba, M. Maurer, P. Vadivelu, *Inorg. Chem.* **2009**, *48*, 10389 – 10396; b) M. R. Bukowski, P. Comba, A. Lienke, C. Limberg, C. Lopez de Laorden, R. Mas-Ballesté, M. Merz, L. Que, Jr., *Angew. Chem.* **2006**, *118*, 3524 – 3528; *Angew. Chem. Int. Ed.* **2006**, *45*, 3446 – 3449.
[30] M. Christmann, *Angew. Chem.* **2008**, *120*, 2780 – 2783; *Angew. Chem. Int. Ed.* **2008**, *47*, 2740 – 2742.
[31] A. N. Biswas, A. Pariyar, S. Bose, P. Das, P. Bandyopadhyay, *Catal. Commun.* **2010**, *11*, 1008 – 1011.
[32] a) T. J. Collins, *Acc. Chem. Res.* **1994**, *27*, 279 – 285; b) A. Marques, M. Marin, M.-F. Ruasse, *J. Org. Chem.* **2001**, *66*, 7588 – 7595.
[33] a) P. Shejwalkar, N. P. Rath, E. B. Bauer, *Dalton Trans.* **2011**, *40*, 7617 – 7631; b) P. Shejwalkar, N. P. Rath, E. B. Bauer, *Molecules* **2010**, *15*, 2631 – 2650; c) M. Lenze, S. L. Sedinkin, N. P. Rath, E. B. Bauer, *Tetrahedron Lett.* **2010**, *51*, 2855 – 2858; d) M. Lenze, E. B. Bauer, *J. Mol. Catal. A* **2009**, *309*, 117 – 123.
[34] A. Diebold, K. S. Hagen, *Inorg. Chem.* **1998**, *37*, 215 – 223.
[35] a) N. M. F. Carvalho, A. Horn, Jr., A. J. Bortoluzzi, V. Drago, O. A. C. Antunes, *Inorg. Chim. Acta* **2006**, *359*, 90 – 98; b) D. Mandon, A. Nopper, T. Litrol, S. Goetz, *Inorg. Chem.* **2001**, *40*, 4803 – 4806.
[36] a) A. Malassa, H. Görls, A. Buchholz, W. Plass, M. Westerhausen, *Z. Anorg. Allg. Chem.* **2006**, *632*, 2355 – 2362; b) C. J. Davies, G. A. Solan, J. Fawcett, *Polyhedron* **2004**, *23*, 3105 – 3114.
[37] a) N. M. F. Carvalho, O. A. C. Antunes, A. Horn, Jr., *Dalton Trans.* **2007**, 1023 – 1027; b) K. Visvaganesan, R. Mayilmurugan, E. Suresh, M. Palaniandavar, *Inorg. Chem.* **2007**, *46*, 10294 – 10306.
[38] J. Cui, M. S. Mashuta, R. M. Buchanan, C. A. Grapperhaus, *Inorg. Chem.* **2010**, *49*, 10427 – 10435.
[39] E. Balogh-Hergovich, G. Speier, M. Réglier, M. Giorgi, E. Kuzmann, Attila Vértes, *Eur. J. Inorg. Chem.* **2003**, 1735 – 1740.
[40] K. Visvaganesan, E. Suresh, M. Palaniandavar, *Dalton Trans.* **2009**, 3814 – 3823.
[41] A. Thibon, J.-F. Bartoli, S. Bourcier, F. Banse, *Dalton Trans.* **2009**, 9587 – 9594.
[42] H. R. Lucas, L. Li, A. A. Narducci Sarjeant, M. A. Vance, E. I. Solomon, K. D. Karlin, *J. Am. Chem. Soc.* **2009**, *131*, 3230 – 3245.
[43] A. C. Mayer, C. Bolm in *Iron Catalysis in Organic Chemistry, 1st ed.* (Ed.: B. Plietker), Wiley-VCH, Weinheim, **2008**, Chapter 3, pp. 73 – 123.
[44] D. W. Blakesley, S. C. Payne, K. S. Hagen, *Inorg. Chem.* **2000**, *39*, 1979 – 1989.
[45] V. Balland, F. Banse, E. Anxolabéhère-Mallart, M. Nierlich, J.-J. Girerd, *Eur. J. Inorg. Chem.* **2003**, 2529 – 2535.
[46] T. Buchen, P. Gütlich, *Inorg. Chim. Acta* **1995**, *231*, 221 – 223.
[47] S. Gosiewska, J. J. L. M. Cornelissen, M. Lutz, A. L. Spek, G. van Koten, R. J. M. Klein Gebbink, *Inorg. Chem.* **2006**, *45*, 4214 – 4227.
[48] J. Kim, R. G. Harrison, C. Kim, L. Que, Jr., *J. Am. Chem. Soc.* **1996**, *118*, 4373 – 4379.
[49] a) M. P. Jensen, A. Mairata i Payeras, A. T. Fiedler, M. Costas, J. Kaizer, A. Stubna, E. Münck, L. Que, Jr., *Inorg. Chem.* **2007**, *46*, 2398 – 2408; b) C. Nguyen, R. J. Guajardo, P. K. Mascharak, *Inorg. Chem.* **1996**, *35*, 6273 – 6281.
[50] M. S. Seo, T. Kamachi, T. Kouno, K. Murata, M. J. Park, K. Yoshizawa, W. Nam, *Angew. Chem.* **2007**, *119*, 2341 – 2344; *Angew. Chem. Int. Ed.* **2007**, *46*, 2291 – 2294.
[51] M. R. Bukowski, H. L. Halfen, T. A. van den Berg, J. A. Halfen, L. Que, Jr., *Angew. Chem.* **2005**, *117*, 590 – 593; *Angew. Chem. Int. Ed.* **2005**, *44*, 584 – 587.
[52] F. Shi, M. K. Tse, Z. Li, M. Beller, *Chem. Eur. J.* **2008**, *14*, 8793 – 8797.
[53] G. A. Russell, *J. Am. Chem. Soc.* **1957**, *79*, 3871 – 3877.
[54] A. Bréhéret, C. Lambeaux, S. Ménage, M. Fontecave, F. Dallemer, E. Fache, J.-L. Pierre, P. Chautemps, M.-T. Averbusch-Pouchot, *C. R. Acad. Sci. Chemistry* **2001**, *4*, 27 – 34.
[55] C. Krebs, D. G. Fujimori, C. T. Walsh, J. M. Bollinger, Jr., *Acc. Chem. Res.* **2007**, *40*, 484 – 492.
[56] M. P. Jensen, M. Costas, R. Y. N. Ho, J. Kaizer, A. Mairata i Payeras, E. Münck, L. Que, Jr., J.-U. Rohde, A. Stubna, *J. Am. Chem. Soc.* **2005**, *127*, 10512 – 10525.
[57] J.-U. Rohde, J. H. In, M. H. Lim, W. W. Brennessel, M. R. Bukowski, A. Stubna, E. Münck, W. Nam, L. Que, Jr., *Science* **2003**, *299*, 1037 – 1039.
[58] A. Decker, J.-U. Rohde, E. J. Klinker, S. D. Wong, L. Que, Jr., E. I. Solomon, *J. Am. Chem. Soc.* **2007**, *129*, 15983 – 15996.
[59] D. H. R. Barton, V. N. Le Gloahec, H. Patin, F. Launay, *New J. Chem.* **1998**, *22*, 559 – 563.
[60] a) X. Baucherel, L. Gonsalvi, I. W. C. E. Arends, S. Ellwood, R. A. Sheldon, *Adv. Synth. Catal.* **2004**, *346*, 286 – 296; b) F. Minisci, F. Recupero, A. Cecchetto, C. Gambarotti, C. Punta, R. Faletti, R. Paganelli, G. Franco Pedulli, *Eur. J. Org. Chem.* **2004**, 109 – 119.
[61] G. Roelfes, M. Lubben, R. Hage, L. Que, Jr., *Chem. Eur. J.* **2000**, *6*, 2152 – 2159.
[62] a) J. Kaizer, M. Costas, L. Que, Jr., *Angew. Chem.* **2003**, *115*, 3799 – 3801; *Angew. Chem. Int. Ed.* **2003**, *42*, 3671 – 3673; b) A. Mairata i Payeras, R. Y. N. Ho, M. Fujita, L. Que, Jr., *Chem. Eur. J.* **2004**, *10*, 4944 – 4953; c) Y. He, J. D. Gordon, C. R. Goldsmith, *Inorg. Chem.* **2011**, *50*, 12651.
[63] F. Namuswe, G. D. Kasper, A. A. Narducci Sarjeant, T. Hayashi, C. M. Krest, M. T. Green, P. Moënne-Loccoz, D. P. Goldberg, *J. Am. Chem. Soc.* **2008**, *130*, 14189 – 14200.
[64] D. M. Pearson, N. R. Conley, R. M. Waymouth, *Organometallics* **2011**, *30*, 1445 – 1453.
[65] D. Pijper, P. Saisaha, J. W. de Boer, R. Hoen, C. Smit, A. Meetsma, R. Hage, R. P. van Summeren, P. L. Alsters, B. L. Feringa, W. R. Browne, *Dalton Trans.* **2010**, *39*, 10375 – 10381.
[66] a) M. C. Bröhmer, S. Mundinger, S. Bräse, W. Bannwarth, *Angew. Chem.* **2011**, *123*, 6299 – 6301; *Angew. Chem. Int. Ed.* **2011**, *50*, 6175 – 6177; b) S. S. Massoud, F. R. Louka, M. Mikuriya, H. Ishida, F. A. Mautner, *Inorg. Chem. Commun.* **2009**, *12*, 420 – 425.
[67] S. J. Lange, H. Miyake, L. Que, Jr., *J. Am. Chem. Soc.* **1999**, *121*, 6330 – 6331.
[68] H. Chowdhury, S. H. Rahaman, R. Ghosh, S. Kumar Sarkar, H.-K. Fun, B. Kumar Ghosh, *J. Mol. Struct.* **2007**, *826*, 170 – 176.

[69] a) D. Wu, *Acta Crystallogr. Sect. E* **2009**, *65*, m1340; b) T. Kajiwara, R. Sensui, T. Noguchi, A. Kamiyama, T. Ito, *Inorg. Chim. Acta* **2002**, *337*, 299 – 307.
[70] C. Panda, M. Ghosh, T. Panda, R. Banerjee, S. S. Gupta, *Chem. Commun.* **2011**, *47*, 8016 – 8018.
[71] K. Barbusiński, *Ecol. Chem. Eng. S* **2009**, *16*, 347 – 358.
[72] J. M. Rowland, M. M. Olmstead, P. K. Mascharak, *Inorg. Chem.* **2002**, *41*, 2754 – 2760.
[73] K. S. Hagen, *Inorg. Chem.* **2000**, *39*, 5867 – 5869.
[74] Bruker Analytical X-Ray, Madison, WI, **2008**.
[75] G. M. Sheldrick, *Acta Crystallogr. Sect. A* **2008**, *64*, 112 – 122.

Received: September 17, 2012
Published online on December 19, 2012